11-12-2021

Non-Adiabatic Excited State Molecular Dynamics Using Ehrenfest and Modulated X-Ray Absorption in Titania

Alexander Matthew Meyer
Louisiana State University and Agricultural and Mechanical College

NON-ADIABATIC EXCITED STATE MOLECULAR DYNAMICS USING EHRENFEST AND MODULATED X-RAY ABSORPTION IN TITANIA

A Dissertation

Submitted to the Graduate Faculty of the
Louisiana State University
and Agricultural and Mechanical College
in partial fulfillment of the
requirements for the degree of
Doctor of Philosophy

in

The Department of Chemistry

by
Alexander Matthew Meyer
B.S., University of California, Irvine, 2010
December 2021

Acknowledgements

Thank you to the people who have helped me along the way, I couldn't have done it without you. I especially appreciate Dr. Kenneth Lopata for allowing me to get to this point, as it wouldn't have been possible without his guidance. I would also like to thank my group members Dr. Adam Bruner, Dr. Pragathi Darapaneni, Dr. Adonay Sissay, and Mengqi Yang for their assistance. It will be difficult to provide an exhaustive list of people who have supported me during this endeavor, so if you've somehow received news of my completion then I extend my gratitude to you.

Table of Contents

Acknowledgements iii

Abstract v

Chapter 1. Introduction 1
1.1 Quantum Mechanics 1
1.2 Applications 1
1.3 Funding Sources 2
1.4 Scope of Dissertation 3

Chapter 2. Theory and Methods 4
2.1 Hartree-Fock 4
2.2 Kohn-Sham Density Functional Theory 9
2.3 Time-Dependent Density Functional Theory 11

Chapter 3. Time Dependent Density Functional Theory with Ehrenfest for Excited State Lifetimes in Materials 12
3.1 Introduction 12
3.2 Theory 14
3.3 Implementation 17
3.4 Results 18

Chapter 4. Simulated Field Modulated X-ray Absorption in Titania 23
4.1 X-Ray Spectroscopy 23
4.2 Simulating X-ray Absorption in Solids 26
4.3 Theory 31
4.4 Results and Discussion 36
4.5 Conclusions 41

Appendix. Copyright Information 43
A.1 Permission to use Chapter 4 text and figures. 43
A.2 Permission to use experimental spectrum of Figure 2 in Chapter 4. . 45

References 46

Vita 60

Abstract

This dissertation contains two separate sections aside from an introduction (Chapter 1): theory and methods (Chapter 2), time dependent density functional theory with Ehrenfest for excited state lifetimes in materials (Chapter 3), and simulated field modulated X-ray absorption in titania (Chapter 4).

Excited state lifetime in insulators and semiconductors can be difficult to compute using quantum chemistry due to their dense excited states. Non-radiative decay in these materials requires the use of non-adiabatic effects to dissipate energy through the means of electron-nuclear coupling such as coherent phonon generation. One method of approaching this challenge in these materials is using Ehrenfest Theorem. Chapter 3 provides a method of correcting the nuclear gradient to include adiabatic effects. This provides an implementation of this correction using expressions from existing quantum chemistry packages. This method is validated using $\mathbf{H}_2^+$ with a minimal basis set**.**

Chapter 4 presents a method of calculating the X-ray absorption near-edge spectra of titania using real-time time-dependent density functional theory. This is done using anatase titania bulk mimicking embedded clusters, which allow for the inclusion of hybrid-functionals without the use of pseudopotentials. These also include spin-orbit coupling in order to get accurate peak-splitting in the spectrum. These were then subjected to different static electric fields and the changes in the electronic structure are examined from changes in the spectrum. These lead to an increase in the peak splitting between t_{2g} peaks and the e_g peaks of the Ti L-edge.

Chapter 1. Introduction

1.1 Quantum Mechanics

Being able to solve for observable quantities of chemicals and their reactions is now a staple when it comes to validating experimental work in chemistry and is used to explain effects from molecular dynamics to spectroscopy. These contribute an explanation for experimental behaviors based on the theories as they are understood, and as a verification tool, it becomes increasingly important to explain what part of the theory contributes to nuances in the results. This can be challenging without explaining some of background that later equations are built on or attempts to solve. In the field of quantum chemistry this can be hampered by wave-particle duality, and while there are multiple ways to account for this, the most popular place to start would be the Schrödinger equation, which dictates the wavefunction of a quantum system.

$$i\hbar\frac{\partial\psi(x,t)}{\partial t} = -\frac{\hbar^2}{2m}\frac{\partial^2}{\partial x^2}\psi(x,t) + V(x,t)\psi(x,t) \tag{1.1}$$

This linear partial differential equation allows the wavefunction $\psi(x,t)$ to be related to observable quantities, with $V(x,t)$ being an external potential. While the equation is exact for one-electron systems, it fails when there is more than one electron. In order to calculate many-electron systems mean-field theory is used.

1.2 Applications

Quantum mechanics provides a very detailed analysis of systems at both small scales and short timescales, ranging from tens of atoms to a few femtoseconds. When done correctly it can replicate electron dynamics and spectrum of the experiments. This provides insight into certain challenges, like non-adiabatic effects and transition metal electron dynamics. Non-adiabatic effects are particularly interesting, since normally they

are used for relaxation dynamics in molecules, thanks to events like surface hopping [1]. While this runs into challenges in materials with a dense manifold of excited states, it can still be done using Ehrenfest dynamics [2]. This is useful in solids when calculating excited state lifetimes in insulators and semiconductors. With continuous improvements in computing power, real-time simulations can also reach longer timescales with larger systems, making this method even more valuable in calculating lifetimes in solid-state materials.

Transition metal systems are some of the more studied systems providing an excellent source of interesting qualities to simulate. Doping, defects, and ligands all change observable quantities in the system like emission and absorption spectroscopy. This makes it excellent at generating and verifying solid-state systems to build upon. Strong and weak field dynamics can also be simulated, even though material breakdown voltages are frequently difficult to match. This provides interesting opportunities to simulate effects like transient absorption, when combined with experiment, provides a real-time view of things like electron dynamics. Strong field effects can also be examined, as insulators and semiconductors can change to metallic around breakdown voltage. This corresponds to the conduction band and valence band approaching one another and eventually overlapping, becoming metallic. The temporary state of the material in this transition is of particular interest.

1.3 Funding Sources

Funded by the U.S. Department of Energy, Office of Science, Basic Energy Sciences, Atomic, Molecular and Optical Sciences under contract number DE-SC0017868. Parts of the research was done with the computational resources provided

by Louisiana State University (http://www.hpc.lsu.edu) and the Louisiana Optical Network Infrastructure (LONI).

1.4 Scope of Dissertation

This dissertation will focus on two separate topics, one being the introduction of non-adiabatic forces to the nuclear motion and the other being the simulating the effects of applied fields on X-ray absorption in titania. The introduction of non-adiabatic forces is done by deriving an appropriate correction to the energy gradient and incorporating it into nuclear motion. This allows for the excited state of the electron to contribute to the potential felt by the nuclei. This is then followed by a brief validation using the H_2^+ atom and a wrapper around the NWCHEM program. In Chapter 4 we present a method for calculating X-ray near edge absorption spectroscopy in titania using RT-TDDFT with the inclusion of spin-orbit effects. This utilizes bulk-mimicking embedded clusters which allow for the inclusion of hybrid functionals and all-electron basis sets. Since spin–orbit coupling is necessary this also functions as a verification of the added ZORA method. This is then expanded by the inclusion of differing static electric fields to change the X-ray absorption spectra.

Chapter 2. Theory and Methods

2.1 Hartree-Fock

In order to provide a more complete explanation of the terms included when solving for later electronic structure calculation, it is important to first define terms, we use the notation from ref Li et al. [2]. Many of the relevant terms can be seen in the Hartree-Fock (HF) method. To get the one electron wavefunction ψ_i and electron energy ϵ_i a version of the Schrödinger equation must be solved using the Fock operator $\hat{f}(i)$.

$$\hat{f}(i)\psi_i = \epsilon_i\psi_i \tag{2.2}$$

Here the Fock operator is:

$$\hat{f}(i) = \hat{h}(i) + \sum_{j=1}^{N/2}\left[2\hat{J}_j(i) - \hat{K}_j(i)\right] \tag{2.3}$$

Here $\hat{h}(i)$ is the one electron Hamiltonian, $\hat{J}_j(i)$ is the Coulomb operator for electron-electron repulsion, and $\hat{K}_j(i)$ is the exchange operator.

$$\begin{aligned}\hat{J}_\nu\psi_\mu(x_1) &= \psi_\mu(x_1)\int dx_2\,\frac{\psi_\mu^*(x_2)\psi_\mu(x_2)}{r_{\mu\nu}}\\ \hat{K}_\nu\psi_\mu(x_1) &= \psi_\nu(x_1)\int dx_2\,\frac{\psi_\nu^*(x_2)\psi_\mu(x_2)}{r_{\mu\nu}}\end{aligned} \tag{2.4}$$

In the both $r_{\mu\nu}$ is the distance between the electrons' positions. The Coulomb operator is the repulsive force felt on the electron by the other electrons in the system. The exchange operator involves the electrons at their own positions, noted by $\psi_\mu(x_1)$ and $\psi_\nu(x_2)$, as well as swapped, noted by $\psi_\mu(x_2)$ and $\psi_\nu(x_1)$.

Another particularly important function to have is the electronic density, which is the density of the total number of electrons in the system as a function of the position. This is defined for Hartree-Fock and DFT as:

$$\rho(\mathbf{r}) = 2\sum_{a=1}^{\mathrm{N}/2} \psi_a^*(\mathbf{r})\psi_a(\mathbf{r}) \tag{2.5}$$

This also means that an integral of the density over all space should result in N, or the total number of electrons.

Here we also run into the problem of not being able to solve for the orbital energy ϵ_i using the wavefunction ψ_i. In order to bypass this we can instead replace our wavefunction with basis sets. In which a linear combination of a finite set of basis functions is used together as a basis set with which to describe the wavefunction ψ_i, provided there are enough basis functions to adequately describe the wavefunction. Here we define our wavefunction as a sum of basis functions ϕ_j which altogether form a basis set.

$$\psi_i = \sum_{j=1}^{\mathrm{K}} c_{ij}\phi_j \tag{2.6}$$

This allows for a solution of the energy ε_i as an eigenvalue of the basis functions ϕ_j as opposed to the wavefunction ψ_i.

$$\sum_{\nu=1}^{K} C_{\mu,i}\langle\phi_\mu|\hat{f}(i)|\phi_\nu\rangle = \varepsilon_i \sum_{\nu=1}^{K} C_{\mu,i}\langle\phi_\mu|\phi_\nu\rangle \tag{2.7}$$

Here the coefficients are written as $C_{\mu,i}$. At this point it is also possible to start defining terms as matrices spanning over the basis function indices μ and ν.

This allows us to replace our previous equations with their basis function counterparts. The electronic density becomes:

$$\rho(\mathbf{r}) = 2\sum_{a=1}^{\mathrm{N}/2}\sum_{\mu\nu} C_{\mu a}^{*} C_{\nu a}\phi_{\mu}^{*}(\mathbf{r})\phi_{\nu}(\mathbf{r}) = \sum_{\mu\nu}\mathbf{P}_{\mu\nu}\phi_{\mu}^{*}(\mathbf{r})\phi_{\nu}(\mathbf{r}) \tag{2.8}$$

Which allows for the definition for the density matrix

$$\mathbf{P}_{\mu\nu} = 2\sum_{a}^{N/2} C_{\mu a}^{*} C_{\nu a} \tag{2.9}$$

The density matrix is useful in that it can completely specify the charge density with a corresponding basis set. It also replaces the coefficient matrix $\mathbf{C}$ with a matrix invariant to transformations performed on the orbitals and by extension to the basis set.

It also becomes possible to define the Fock matrix $\mathbf{F}$ using basis functions

$$\mathbf{F}_{\mu\nu} = \langle\phi_{\mu}|\hat{f}(i)|\phi_{\nu}\rangle \tag{2.10}$$

The Fock matrix can then be expanded the same way as the Fock operator was above. With the Hamiltonian $\hat{h}(i)$ and two-electron contributions from $\hat{J}_j(i)$ and $\hat{K}_j(i)$ also acting upon basis functions.

$$\mathbf{F}_{\mu\nu} = \langle\phi_{\mu}|\hat{h}(i)|\phi_{\nu}\rangle + \sum_{j=1}^{\mathrm{N}/2}\langle\phi_{\mu}|2\hat{J}_j(i) - \hat{K}_j(i)|\phi_{\nu}\rangle \tag{2.11}$$

Here we can refer to $\langle\phi_{\mu}|\hat{h}(i)|\phi_{\nu}\rangle$ as the core Hamiltonian $\mathbf{H}_{\boldsymbol{\mu\nu}}^{\mathrm{core}}$ and the coulomb and exchange operators become the two-electron contribution $\mathbf{G}_{\mu\nu}$

$$\sum_{j=1}^{\mathrm{N}/2}\langle\phi_{\mu}|2\hat{J}_j(i) - \hat{K}_j(i)|\phi_{\nu}\rangle = \sum_{\lambda\sigma}\mathbf{P}_{\mu\nu}\left[(\mu\nu|\lambda\sigma) - \frac{1}{2}(\mu\sigma|\lambda\nu)\right] = \mathbf{G}_{\mu\nu} \tag{2.12}$$

So the Fock matrix can be reduced into the much simpler:

$$\mathbf{F}_{\mu\nu} = \mathbf{H}_{\boldsymbol{\mu\nu}}^{\mathrm{core}} + \mathbf{G}_{\mu\nu} \tag{2.13}$$

This means that the Fock matrix can be expressed as a function of the density matrix and therefore the coefficient matrix. Lastly, since the basis sets are not necessarily orthogonal to each other an overlap matrix is produced

$$\mathbf{S}_{\mu\nu} = \langle \phi_\mu | \phi_\nu \rangle \tag{2.14}$$

This allows for the original energy ϵ to be rewritten with the corresponding matrix representations.

$$\mathbf{FC} = \mathbf{SC}\epsilon \tag{2.15}$$

Solving this could be made much simpler if the overlap matrix was equal to the identity matrix and could therefore be removed. Then the coefficient matrix could be found by diagonalizing the Fock matrix.

Transforming the overlap matrix into the identity matrix is done using orthogonalization. Although this is hampered by the fact that the overlap matrix isn't necessarily invertible, which means canonical orthgonalization needs to be used. The transform matrix $\mathbf{X}$ is defined as:

$$\mathbf{X} = \mathbf{U}\boldsymbol{s}^{-\mathbf{1/2}} \tag{2.16}$$

Where the unitary matrix $\mathbf{U}$ is used to diagonalize $\mathbf{S}$ into the overlap eigenvalues $\mathbf{s}$.

$$\mathbf{U}^\dagger \mathbf{S} \mathbf{U} = \mathbf{s} \tag{2.17}$$

This allows for the transformation

$$\mathbf{X}^\dagger \mathbf{S} \mathbf{X} = \mathbf{1} \tag{2.18}$$

With the transform matrix available it becomes possible to create an orthonormal basis set and transform our matrices into the orthonormal basis. This allows for the orthogonal form of the coefficient matrix to be defined as

$$\mathbf{C}' = \mathbf{X}^{-1}\mathbf{C} \tag{2.19}$$

The orthogonal Fock matrix is also transformed into the orthonormal basis by

$$\mathbf{F}' = \mathbf{X}^{\dagger}\mathbf{F}\mathbf{X} \tag{2.20}$$

Now the energy can be rewritten again in the orthonormal basis as

$$\mathbf{F}'\mathbf{C}' = \mathbf{C}'\epsilon \tag{2.21}$$

At this point the Self-Consistent Field (SCF) method allows for solving the energy.

The SCF method refers to the process of iteratively solving to a point that all of the orbitals are eigenvectors of the Fock matrix. This begins with first defining the system, in terms of positions, nuclei, basis sets, and number of spin-up and spin-down electrons. From the system the core Hamiltonian, two-electron, and overlap matrices can be solved, followed by diagonalizing the overlap matrix to obtain the canonical transformation matrix. At this point a guess for the density matrix must be made from the coefficients matrix, while there are a number of ways to do this a simple example would be to solve the Fock matrix with the coulomb operator set to zero, functionally ignoring electron repulsion. Regardless of how the guess is constructed, it is used to start an iterative loop, the first step of which is using our generated density matrix to solve for the Fock matrix. From this the canonical transformation matrix can be used to transform the newly created Fock matrix into the orthonormal basis which can be used to solve for the transformed coefficient matrix and energy. The coefficient matrix can then be transformed back out of

the orthonormal basis to create a new iteration of the density matrix. At this point if the new density matrix is different from the previous density matrix the loop is restarted, using the new density matrix to generate a newer density matrix. If these iterations of the density matrix become sufficiently close the loop can be considered self-consistent, and the final coefficient matrix can be used to solve for observable properties.

2.2 Kohn-Sham Density Functional Theory

While solving for a single hydrogen atom can be done analytically, including a third body or more makes the problem currently unsolvable. And while there are a number of approximations to circumvent this challenge, the one foundational to DFT are the Kohn-Sham equations [3]. These provide some corrections to the Hartree-Fock method, namely the exchange-correlation function. The Kohn-Sham equation replaces any number of electrons with one non-interacting density cloud containing all of them, which can simplify a many-body problem back into a two-body one. The Kohn-Sham wavefunction is similar to the one-electron Schrödinger equation and must obey the equation,

$$\left(-\frac{\hbar^2}{2m}\nabla^2 + v_{\text{eff}}(\mathbf{r})\right)\phi_i(\mathbf{r}) = \varepsilon_i\phi_i(\mathbf{r}) \tag{2.22}$$

Where ε_i is the energy of the Kohn-Sham orbital ϕ_i, and v_{eff} is the Kohn-Sham potential which has a dependence on the electronic density given by $\rho(\mathrm{r})$.

$$\rho(\mathbf{r}) = \sum_i^N |\phi_i(\mathbf{r})|^2 \tag{2.23}$$

It should be noted that this represents a non-interacting system of electrons. The challenge becomes solving or approximating the Kohn-Sham potential, which is dependent on three separate parts:

$$v_{\text{eff}}(\mathbf{r}) = v_{\text{ext}}(\mathbf{r}) + v_{\text{Hartree}}(\mathbf{r}) + v_{\text{XC}}(\mathbf{r}) \tag{2.24}$$

Here the effective potential is split into an external potential, the Hartree potential, and the exchange correlation.

$$v_{\text{ext}}(\mathbf{r}) = \sum_{\alpha} v_{\alpha}(\mathbf{r} - \mathbf{R}_{\boldsymbol{\alpha}}) \tag{2.25}$$

The external potential is just an external potential or number of potentials being applied to the electron.

$$v_{\text{Hartree}}(\mathbf{r}) = \int dr' \frac{\rho(\mathbf{r}')}{|\mathbf{r} - \mathbf{r}'|} \tag{2.26}$$

Which is the Hartree potential as a function of the density.

$$v_{\text{XC}}(\mathbf{r}) = \frac{\delta E_{XC}}{\delta \rho(\mathbf{r})} \tag{2.27}$$

Here E_{XC} is the exchange correlation energy and is supposed to take into account any other ground state energies that are not included in the ground state energy expression, which can now be expressed as:

$$E(\rho) = T_s(\rho) + \int d\mathbf{r}\, v_{\text{ext}}(\mathbf{r})\rho(\mathbf{r}) + \tfrac{1}{2}\iint d\mathbf{r}\, d\mathbf{r}' \frac{\rho(\mathbf{r})\rho(\mathbf{r}')}{|\mathbf{r} - \mathbf{r}'|} + E_{XC}(\rho) \tag{2.28}$$

Where $T_s(\rho)$ is the Kohn Sham kinetic energy, given by:

$$T_s(\rho) = \sum_{i=1}^{N} \int d\mathbf{r}\, \phi_i^*(\mathbf{r}) \left(\frac{\hbar^2}{2m}\nabla^2\right) \phi_i(\mathbf{r}) \tag{2.29}$$

The remaining expressions are the energy of the external potential, the Hartree energy, and the Exchange correlation energy.

$$E_{\text{DFT}} = \sum_{i}^{\text{OCC}} \varepsilon_i - \int dr \left[\frac{1}{2} v_{\text{Hartree}}(\mathbf{r}) + v_{\text{XC}}(\mathbf{r})\right] \rho(\mathbf{r}) + E_{\text{XC}} \tag{2.30}$$

This method is further expanded into the time domain by the time-dependent Kohn-Sham equations utilizing the Runge-Gross theorem[4].

$$i\frac{\partial \phi_i(\mathbf{r},t)}{\partial t} = \left[-\frac{1}{2}\nabla^2 + \upsilon_{\mathrm{KS}}(\mathbf{r},t)\right]\phi_i(\mathbf{r},t) \tag{2.31}$$

2.3 Time-Dependent Density Functional Theory

Building upon the time-dependent Kohn-Sham equations, DFT can be similarly extended into the time domain with time-dependent density functional theory (TDDFT). Still satisfying the Kohn-Sham equations above the Schrödinger equation becomes defined by:

$$i\frac{\partial \psi_i(\mathbf{r},t)}{\partial t} = \left[-\frac{1}{2}\nabla^2 + \upsilon_{\mathrm{ext}}(\mathbf{r},t) + \int d\mathbf{r}'\frac{\rho(\mathbf{r}')}{|\mathbf{r}-\mathbf{r}'|} + \upsilon_{\mathrm{XC}}(\mathbf{r},t)\right]\psi_i(\mathbf{r},t) \tag{2.32}$$

This assumes a DFT functional that is adiabatic (local in time). The exchange correlation functional depends on a complete history of the density, however for practical calculations, adiabatic functionals are almost always used [5, 6]. TDDFT can be subdivided into two regimes, namely linear-response (LR) and real-time (RT), whereas LR-TDDFT solves for excitations in the frequency domain by using Davidson iterations. RT-TDDFT is similar to LR-TDDFT, but instead solves for excited states by integrating the time-dependent Kohn-Sham equations in the time domain [7, 8]. This allows for the computation of spectroscopic properties as well as time-resolved response to excitations or changes in the system. Provided a long enough time-scale and a fine enough time-step, excitations can be calculated using a Fourier transform.

Chapter 3. Time Dependent Density Functional Theory with Ehrenfest for Excited State Lifetimes in Materials

3.1 Introduction

Full quantum mechanical molecular dynamics and time evolution for chemical properties and excited state processes, generally requires a full solution of the time-dependent Schrödinger equation for the entire system, however in practice this is not computationally feasible. One method of simplifying the solution to the system is the Born-Oppenheimer approximation. This stems from the fact that the nuclei and electrons are vastly different in mass, so we should be able to solve for the electronic wavefunction with fixed nuclear positions. This simplifies the problem by separating the total wavefunction of the system into its nuclear and electronic portions each solved in their own timescale. While effective this limits the effects electrons can impart upon the nuclei. Their motion is only propagated with a snapshot of the other in mind effectively simplifying the entire motion of electrons between nuclear propagation steps to a single frame, which is usually the ground state electronic wavefunction. The assumption is that any appreciable nuclear change will happen at a timescale so much larger than the electronic propagation that the electrons will relax down to the ground state before the nuclei are propagated again. This is often also reasonable because in an adiabatic system, small enough changes in the nuclear position will yield the same electronic state.

There are many cases where this assumption is no longer valid, including most non-adiabatic processes. Especially in cases where electrons move slower, the timescales will approach similar values and the back reaction of the electrons upon the nuclei can’t be ignored. These are common in both transition state systems and during chemical reactions. In systems that undergo photochemical reactions, since the electrons

are the one accepting the energy of the photon and exciting, it is frequently their excited states that lead to changes in the molecule. In many situations where the Born-Oppenheimer approximation breaks down it becomes necessary to choose a more applicable method.

In crystal lattices and solid state materials analogous processes occur energy loss pathways, where excited electrons couple to lattice motion [9]. Understanding these dynamics is important to effectively predict the excited state lifetimes of these systems which continually display a transfer of energy from the excited state electrons into the lattice. While there is ongoing research into this challenge, Ehrenfest provides a simple method for simulating these systems, trading accuracy for efficiency for solid state materials[10]. Plane waves are also an option when doing these simulations, and while accurate, they run into challenges when dealing with defects in the lattice and have difficulty establishing reasonable concentrations of defects or dopants.

Surface Hopping and Ehrenfest are two of the more common methods applied to non-adiabatic systems [11]. Surface Hopping propagates along the potential energy surface of one adiabatic state with ”hops” between the current state and nearby states depending on coupling between the states [12]. In situations where there is a large difference in adiabatic states that only approach briefly, this method is very convenient, since a number of trajectories run at once and can simulate a system that moves between the ground and excited states freely. Unfortunately it requires calculations of the nearest adiabatic surfaces, making it expensive in systems with of dense states. Ehrenfest overcomes this problem by propagating along a mean field of states allowing a number of states to be averaged into a single state provided they are close enough in energy [2].

It is less accurate when trying to average over states with large energy gaps between the states, and can give unrealistic results when calculating the conformations of different molecules. Since this work is intended to be used in solid state systems such as insulators or semiconductors with high densities of states it is cheaper and can be more accurate to use Ehrenfest. This is particularly convenient if there is a dense manifold of similarly shaped energy surfaces and the simulation can represent a realistic average of states. Under the conditions of a density of excited states we can expect Ehrenfest method to be not only reasonably accurate, but also computationally efficient, reducing the need to simulate every state in the manifold. When combined with TDDFT it provides a good balance of accuracy and efficiency when applied to this system. Essentially this can be implemented by correcting the forces in a traditional Born-Oppenheimer molecular dynamics calculation of the electronic gradient upon the nuclei to account for excited state character.

3.2 Theory

Here is discussed the technical approach for Ehrenfest with atom centered basis sets within TDDFT, which are well suited to simulating non-adiabatic processes in doped solids using hybrid DFT functionals and cluster simulations (See chapter 4) [13]. In this section we adapt the results from Li et al. [2]. In Born-Oppenheimer Molecular Dynamics the movement of the nuclei is based on the force imparted by the energy gradient. This is correct for systems where the electrons reside in the ground state and uses that fact to simplify the energy gradient. Ehrenfest molecular dynamics however, requires a gradient that takes into account the electronic excited state. This means the full expression for the gradient is needed to propagate the nuclei. We start with the expression for energy in the

atomic orbital basis set, where $\mathbf{F}$ is the Fock matrix in the atomic orbital basis, $\mathbf{P}$ is the density matrix in the atomic orbital basis, and v_{NN} is the nuclear-nuclear interaction.

$$\begin{aligned} E &= Tr[\mathbf{F}(\mathbf{P})\mathbf{P}] + v_{NN} \\ &= Tr\left[\mathbf{hP} + \frac{1}{2}\mathbf{G}(\mathbf{P})\mathbf{P}\right] + v_{NN} \end{aligned} \tag{3.1}$$

The gradient in the d direction on atom a is then.

$$\frac{\partial E}{\partial R_a^d} = Tr\left[\frac{\partial \mathbf{h}}{\partial R}\mathbf{P} + \mathbf{h}\frac{\partial \mathbf{P}}{\partial R} + \frac{1}{2}\frac{\partial \mathbf{G}}{\partial R}\mathbf{P} + \frac{1}{2}\mathbf{G}\frac{\partial \mathbf{P}}{\partial R}\right] + \frac{\partial v_{NN}}{\partial R} \tag{3.2}$$

$$= Tr\left[\frac{\partial \mathbf{h}}{\partial R}\mathbf{P} + \frac{1}{2}\frac{\partial \mathbf{G}}{\partial R}\mathbf{P}\right] + Tr\left[\mathbf{F}\frac{\partial \mathbf{P}}{\partial R}\right] + \frac{\partial v_{NN}}{\partial R} \tag{3.3}$$

Here $\mathbf{h}$ is the core part of the Fock matrix and represents the kinetic energy and the one electron portion while $\mathbf{G}$ is the two-electron portion. Here is also where we need to solve for $\mathrm{Tr}\left[\mathbf{F}\frac{\partial \mathbf{P}}{\partial \mathrm{R}}\right]$. Here it is also important to mention that any partial derivatives at this point should be attempted to be converted into something in terms of $\frac{\partial \mathbf{S}}{\partial \mathrm{R}}$ where $\mathbf{S}$ is the overlap matrix. This enables evaluation of the matrix elements in terms of the atomic orbital basis, which is the most convenient form for implementing in an electronic structure code. This is accomplished by first solving $\frac{\partial \mathbf{P}}{\partial \mathrm{R}}$, which is substituted into $\mathrm{Tr}\left[\mathbf{F}\frac{\partial \mathbf{P}}{\partial \mathrm{R}}\right]$ and solved in terms of $\frac{\partial \mathbf{S}}{\partial \mathrm{R}}$. This method yields.

$$Tr\left[\mathbf{F}\frac{\partial \mathbf{P}}{\partial R}\right] = Tr\left[\mathbf{P}'\mathbf{F}'\mathbf{Y}^{\dagger}\frac{\partial \mathbf{X}}{\partial R} + \mathbf{F}'\mathbf{P}'\frac{\partial \mathbf{X}^{\dagger}}{\partial R}\mathbf{Y}\right] \tag{3.4}$$

Where:

$$\mathbf{F}'\mathbf{P}' = \mathbf{P}'\mathbf{F}' - [\mathbf{P}', \mathbf{F}'] \tag{3.5}$$

Here $\mathbf{X}$ is the canonical transform matrix. For Born-Oppenheimer molecular dynamics, we make use of the fact that $[\mathbf{F}, \mathbf{P}] = 0$ to remove a portion of the solution that will equal 0 for the ground state. Which yields:

$$Tr\left[\mathbf{F}\frac{\partial \mathbf{P}}{\partial R}\right] = -Tr\left[\mathbf{PFP}\frac{\partial \mathbf{S}}{\partial R}\right] \tag{3.6}$$

Unfortunately, this method makes use of the fact that $[\mathbf{F}, \mathbf{P}] = 0$ which is no longer valid in the excited state. Without exploiting this characteristic another term is appended onto the end of the previous solution, which requires its own method of solution.

Solving with the excited state in mind yields.

$$\begin{aligned} Tr\left[\mathbf{F}\frac{\partial \mathbf{P}}{\partial R}\right] &= -Tr\left[\mathbf{PFP}\frac{\partial \mathbf{S}}{\partial R}\right] + Tr\left[[\mathbf{P}', \mathbf{F}']\mathbf{X}^{\dagger}\frac{\partial \mathbf{S}}{\partial R}\mathbf{X}\mathbf{P}'\right] \\ &+ Tr\left[[\mathbf{P}', \mathbf{F}']\mathbf{X}^{\dagger}\frac{\partial \mathbf{S}}{\partial R}\mathbf{X} + [\mathbf{P}', \mathbf{F}']\mathbf{X}^{\dagger}\mathbf{S}\frac{\partial \mathbf{X}}{\partial R}\right] \end{aligned} \tag{3.7}$$

This contains the original $-Tr\left[\mathbf{PFP}\frac{\partial \mathbf{S}}{\partial R}\right]$ term as well as two additional terms that would have been ignored in the ground state. This is then appended to the gradient of nuclei to account for electron effects on the nuclei. In this project it is subsequently used in the velocity verlet along with the gradient provided by NWChem [14]. It can also be substituted into the overall gradient for a complete expression of the gradient.

$$\begin{aligned} \frac{\partial E}{\partial R_a^d} &= Tr\left[\frac{\partial \mathbf{h}}{\partial R}\mathbf{P} + \frac{1}{2}\frac{\partial \mathbf{G}}{\partial R}\mathbf{P}\right] - Tr\left[\mathbf{PFP}\frac{\partial \mathbf{S}}{\partial R}\right] + Tr\left[[\mathbf{P}', \mathbf{F}']\mathbf{X}^{\dagger}\frac{\partial \mathbf{S}}{\partial R}\mathbf{X}\mathbf{P}'\right] \\ &+ Tr\left[[\mathbf{P}', \mathbf{F}']\mathbf{X}^{\dagger}\frac{\partial \mathbf{S}}{\partial R}\mathbf{X} + [\mathbf{P}', \mathbf{F}']\mathbf{X}^{\dagger}\mathbf{S}\frac{\partial \mathbf{X}}{\partial R}\right] + \frac{\partial v_{NN}}{\partial R} \end{aligned} \tag{3.8}$$

Once all the matrices are found the additional terms can be added to the existing gradient, this negates the need to recalculate the gradient, as the electronic effects can be implemented by adding the additional terms to the ground state gradient routine. Thus,

the excited state forces on the atom can be computed from the instantaneous density using the standard ground state force routine from geometry optimization with a "correction" term relating to the $\frac{\partial \mathbf{S}}{\partial R}$ and $\frac{\partial \mathbf{X}}{\partial R}$ matrices.

3.3 Implementation

In this section we discuss a proof of principle implementation of this technique in NWChem [11]. The integration of the electronic wavefunction is more difficult when done using atom centered basis sets when compared to a grid-based approach. It is therefore in the interest of time that TDDFT is used to solve for the necessary matrices, this provides a canonical transform $\mathbf{X}$ matrix, an overlap $\mathbf{S}$ matrix, a Fock $\mathbf{F}$ matrix, and a ground state gradient $\frac{\partial E}{\partial R_a^d}$ matrix. These matrices are taken from NWChem at every iteration of this method to simplify the calculations. During each iteration the new positions of the two hydrogens are replaced and NWChem is rerun to establish our matrix values. At this step the density matrix is propagated using the Runge-Kutta (RK4) [9]. RK4 requires the $\frac{d\mathbf{P}}{dt}$ matrix.

$$\frac{d\mathbf{P}}{dt} = -i[\mathbf{F}', \mathbf{P}'] \tag{3.9}$$

This is done by using the $\mathbf{X}$ matrix to generate the $\mathbf{Y}$ transform matrix and provide both of their corresponding transforms in the orthogonal (or molecular) basis, $\mathbf{X}'$ and $\mathbf{Y}'$ respectively. These are then used to generate $\mathbf{P}'$ and $\mathbf{F}'$ which are the $\mathbf{P}$ and $\mathbf{F}$ matrices in the orthogonal basis, using the two transform matrices. Utilizing the $\mathbf{P}'$ and $\mathbf{F}'$ matrices for $\frac{d\mathbf{P}}{dt}$ which can then be used to propagate the electronic density to the next timestep using RK4 [2]. By repeating this the program propagates the electronic density alongside the nuclear movement. At this point the nuclei are only responding to a ground state

electronic density and the other nuclei, where it needs to react the electronic density that has been propagated. Here is also where the additional terms to the gradient $\frac{\partial E}{\partial R_a^d}$ matrix need to be generated. The $\mathbf{P}'$, $\mathbf{F}'$, $\mathbf{X}$, $\mathbf{X}^{\dagger}$, $\mathbf{X^{-1}}$, $\boldsymbol{S^{-1}}$ and $\mathbf{S}'$ matrices have already been solved for except for $\frac{\partial \mathbf{S}}{\partial R}$ and $\frac{\partial \mathbf{X}}{\partial R}$. They can be solved by varying the nuclear positions in TDDFT and using it to generate a finite derivative, or by relating $\frac{\partial \mathbf{S}}{\partial R}$ and $\frac{\partial \mathbf{X}}{\partial R}$ from derivatives of the atomic orbital basis functions. With all the previous matrices it becomes possible to solve for the additional terms of $\frac{\partial E}{\partial R_a^d}$. With the additional terms of the gradient solved it can be applied to the gradient provided by NWChem. This full gradient is then used as a force in the acceleration of the velocity verlet [15].

3.4 Results

H_2^+ with minimal basis set is used to demonstrate the validity of the correction term that was developed. Minimal basis sets were used to save time and to simplify the process. It is also useful at this point to generate a potential energy plot of the molecule in question so we can have an expectation of the behaviors that should be demonstrated.

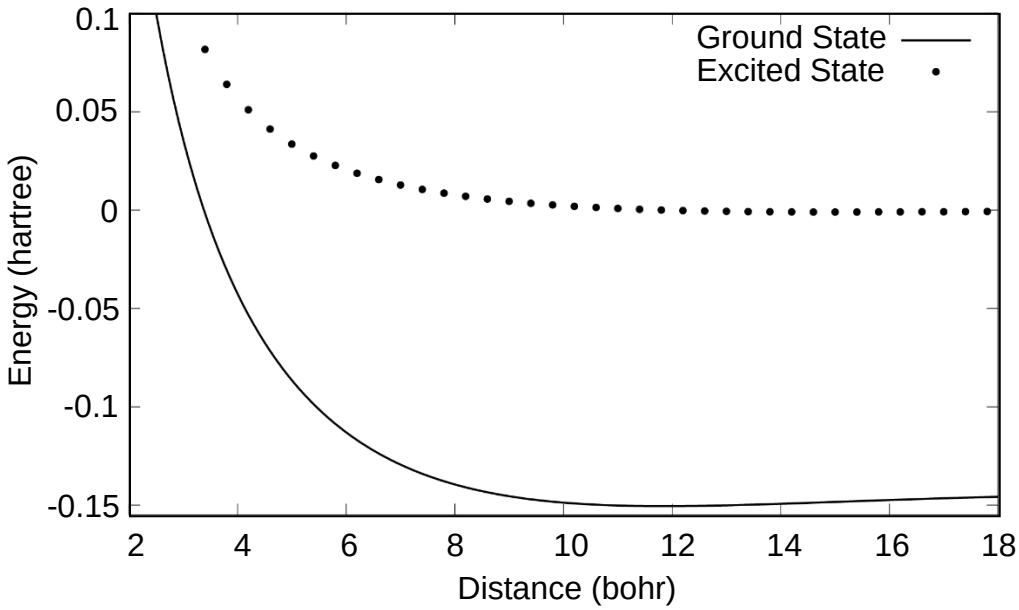

Figure 3.1: Potential energy surfaces of the ground and first excited state of H_2^+ with a minimal basis.

Here in Figure 3.1 the equilibrium distance between the two hydrogens is around 12 Bohr for this simulation. This is not the equilibrium distance found in experiments but is the consequence of using a minimal basis set. Also, while the ground state has a minimum, the first excited state lacks one, meaning that when excited the two hydrogens can be expected to dissociate.

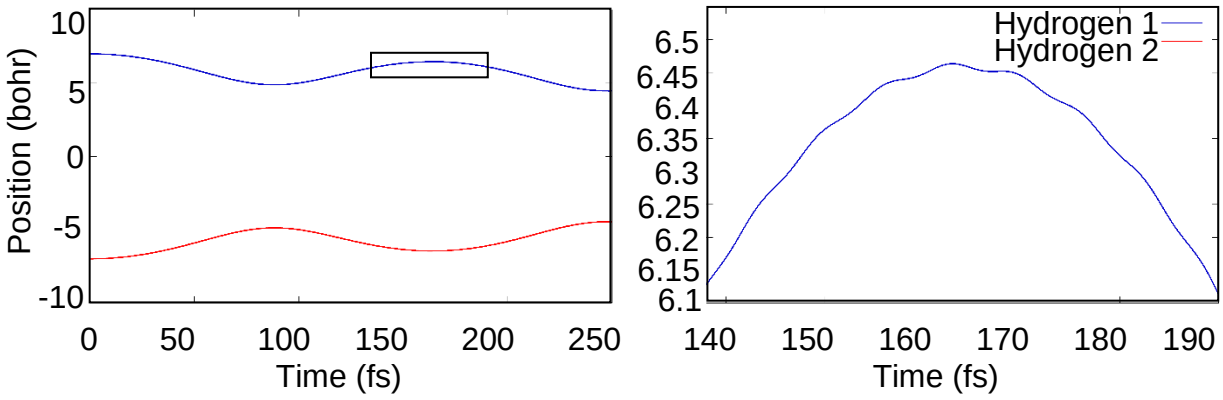

Figure 3.2: Dynamics of the H_2^+ molecule in the ground state, with zoomed in section of interest showing the faster ripples caused by the electronic wavefunction during the nuclear motion.

Figure 3.2 shows the propagation the hydrogen molecule through time when started displaced from the equilibrium position. Here the atoms are shown oscillating around one another. There is a slight overall drift toward one another, but this can be an effect of degradation in the integrator, which can be improved by decreasing the time step, using other integrators, or both. The effects of the excited state correction are seen in the form of ripples along the Hydrogen's trajectory. It is accounting for the tug of the electron as it evolves with respect to nuclear motion.

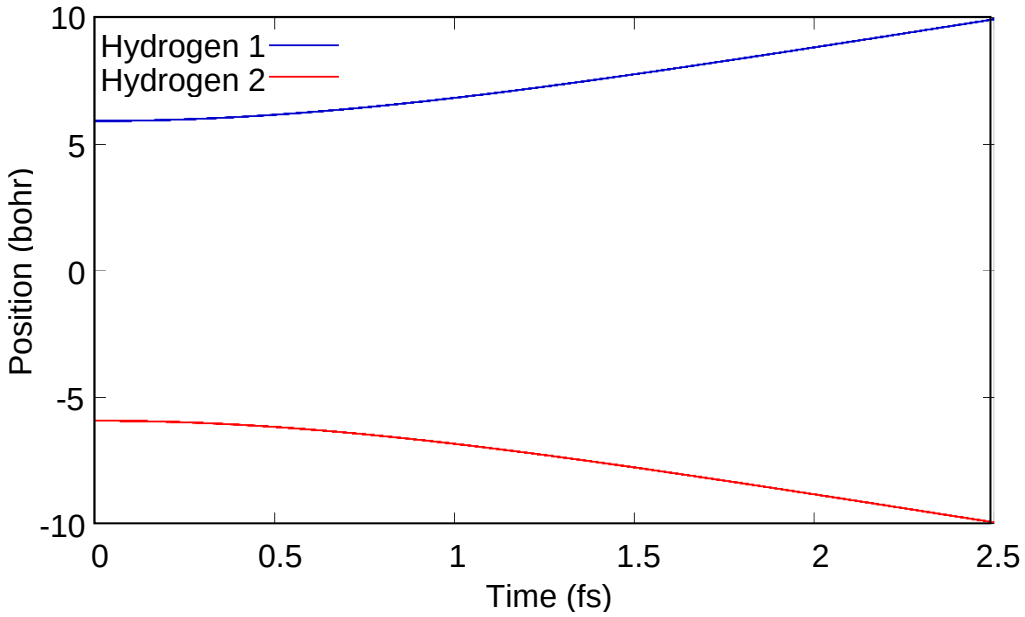

Figure 3.3: Excitation of the H_2^+ molecule in the excited state causes dissociation.

As demonstrated in Figure 3.3 when provided with a superposition of the ground and excited state density the molecule dissociates [16]. This result is physical and expected from the potential energy surfaces. The approach shown here would allow for a non-adiabatic addition to the gradient, allowing for the development of a more robust Ehrenfest code within TDDFT for many-electron systems. The results show that even for the simple hydrogen molecule there is an effect caused by the electron dynamics. This effect can clearly be seen by the smaller oscillations on the hydrogen atoms' trajectories. The results may have been skewed but the average distance between the atoms, while questionable, were expected due to the minima provided in the potential energy surface. While excited it also behaved according to expectations, having the hydrogen molecule split.

This method has only been demonstrated in the test cases provided above, but set the stage for future work. Implementation into a TDDFT code or when combined with surface hopping methods will allow for calculation of non-adiabatic effects on the nuclei.

Following testing, it should be able to propagate the excitation of a crystalline solid such as diamond. It should also be able predict the excited states coupled to various phonon modes, and when done in combination with clusters embedded in a harmonic oscillating lattice, also be able to follow the transfer of excitation to generation of particular phonon modes. This allows for the calculation of nuclear motion in solids from purely electronic processes.

Chapter 4. Simulated Field Modulated X-ray Absorption in Titania

4.1 X-Ray Spectroscopy

X-ray spectroscopy is the analysis of materials using X-ray excitation, which occurs when an electron from the inner core shells of an electron is promoted to a low-lying virtual orbital upon excitation [17]. Due to local nature of the core electrons and differences in the energy level allows for specific analysis of the composition of materials. When combined with short femtosecond pulses it can also be used to probe ultrafast electronic processes [18]. X-ray spectroscopy includes a number of techniques, including near edge X-ray absorption fine structure (NEXAFS), X-ray photoemission spectroscopy (XPS), X-ray emission spectroscopy (XES), and resonant inelastic X-ray scattering (RIXS), each denoting the particular process being examined. NEXAFS is synonymous with X-ray absorption near edge structure (XANES) and corresponds to the measurement of the initial photon as well as the photoelectron, emitted electron, or fluorescent photon. XANES can be particularly useful in speciation, detecting the oxidation state, as well as examining any ligand or solvation effects.

XANES spectroscopy can generally be filtered into different “edges” each with three different regions. The edges are separated by which of the core electrons are being excited, with the 1s electrons composing the K-edge, the 2s and 2p electrons forming the L-edge, and 3s, 3p, and 3d electrons forming the M-edge. The L and M edges can further be subdivided into L_I, L_{II}, and L_{III} depending on which specific electron from the 2s and 2p orbitals are being excited, and M_1 to M_5 depending on the 3s, 3p, and 3d electrons. The K, L, and M edges are also divided into general regions depending on where they are relative to the onset edge. Features before the onset edge are referred to as “pre-edge”,

being before the rising peak in the spectrum, these are usually bound state transition, for example a 1s to unfilled 3d orbital, while this is forbidden by dipole selection rules it can be seen nonetheless due to orbital mixing and quadrupole coupling. The rising edge region and its immediate vicinity can contain a few different transitions that aren't easy to tell apart, and contain transitions that are dipole allowed making more intense peaks. The regions farther from the edge are referred to as extended X-ray absorption fine structure (EXAFS) and contained information from the scattering of the excited photoelectron with nearby non-excited electrons.

In K and L-edge XAS the nature of being a core electron so close to the nucleus introduces the need for spin-orbit coupling. Since the nuclear magnetic field affects the electrons based on their spin, electrons of the same orbital will experience slightly different drag due to their dipole and end up splitting slightly, much like how electrons are split by an external magnetic field in the Zeeman Effect. Capturing these spin–orbit effects is necessary to simulate L_{II} and L_{III} edges. For a single hydrogen atom this effect can be demonstrated as a perturbation to the Hamiltonian in the form of a Larmor precession and Thomas correction, in which the spin magnetic moment of the electron experiences torque when in a magnetic field. A rigorous method of implementation of spin-orbit coupling can be found utilizing a two-component electrons-only Dirac equation as it applies to DFT, since the Dirac equation includes relativistic effects [19, 20].

$$\left(\beta mc^2 + c\sum_{n=1}^{3}\alpha_n p_n\right)\psi(x,t) = i\hbar\frac{\partial\psi(x,t)}{\partial t} \tag{4.33}$$

In Dirac's equation p_n are the momentum operator while c is the speed of light and $\hbar$ is the reduced Planck constant. Here β is a 2x2 matrix with 1 and -1 on the diagonal, while α_n instead has Pauli matrices σ_n on the off diagonals.

$$\sigma_1 = \begin{pmatrix} 0 & 1 \\ 1 & 0 \end{pmatrix} \ \sigma_2 = \begin{pmatrix} 0 & -i \\ i & 0 \end{pmatrix} \ \sigma_3 = \begin{pmatrix} 1 & 0 \\ 0 & -1 \end{pmatrix} \tag{4.34}$$

It is also important to note that the wavefunction ψ is four-component, which means that it is a superposition of spin-up and spin-down electrons and positrons in the form of a bispinor. A spinor is a representation of a particle including the eigenstates of the spin angular momentum as a column matrix, this can be written generally as:

$$\chi = \begin{pmatrix} \langle +|A\rangle \\ \langle -|A\rangle \end{pmatrix} = \begin{pmatrix} c_+ \\ c_- \end{pmatrix} = c_+\chi_+ + c_-\chi_- \tag{4.35}$$

Since the positrons aren't necessary in the representation of the electrons the Dirac equation is block-diagonalized into the two-component form: There are a few ways of doing this, namely the second-order Douglas-Kroll-Hess (DKH2) method, the Barysz-Sadlej-Snijders (BSS) method, and the exact two-component (X2C) method, but in this work the zeroth-order regular approximation (ZORA) is used.

$$\begin{pmatrix} \boldsymbol{V} & \boldsymbol{T} \\ \boldsymbol{T} & \left(\frac{1}{4c^2}\boldsymbol{W} - \boldsymbol{T}\right) \end{pmatrix} \begin{pmatrix} \boldsymbol{C}_L^+ & \boldsymbol{C}_L^- \\ \boldsymbol{C}_S^+ & \boldsymbol{C}_S^- \end{pmatrix} = \begin{pmatrix} \boldsymbol{S} & 0 \\ 0 & \frac{1}{2c^2}\boldsymbol{T} \end{pmatrix} \begin{pmatrix} \boldsymbol{C}_L^+ & \boldsymbol{C}_L^- \\ \boldsymbol{C}_S^+ & \boldsymbol{C}_S^- \end{pmatrix} \begin{pmatrix} \boldsymbol{\varepsilon}^+ & 0 \\ 0 & \boldsymbol{\varepsilon}^- \end{pmatrix} \tag{4.36}$$

This is done using Here $\boldsymbol{V}$ is the one electron potential energy operator matrix, $\boldsymbol{T}$ is the non-relativistic kinetic energy matrix, $\boldsymbol{S}$ is the overlap matrix, and $\boldsymbol{W}$ is the relativistic potential matrix. The components of the relativistic potential matrix are given by:

$$W_{ij} = \langle \chi_i | \vec{\sigma} \cdot \vec{p} \mathcal{V} \vec{\sigma} \cdot \vec{p} | \chi_j \rangle \tag{4.37}$$

Where $\vec{\sigma}$ is a vector containing the Pauli matrices and $\vec{p}$ is the linear momentum vector. In this case $\{\chi_i\}$ are spinors for the electrons.

$$\tilde{\mathbf{H}} = \left(\mathbf{U}^{LL,\dagger}\ \mathbf{U}^{SL,\dagger}\right) \begin{pmatrix} \boldsymbol{V} & \boldsymbol{T} \\ \boldsymbol{T} & \left(\frac{1}{4c^2}\boldsymbol{W} - \boldsymbol{T}\right) \end{pmatrix} \begin{pmatrix} \mathbf{U}^{LL} \\ \mathbf{U}^{SL} \end{pmatrix} \tag{4.38}$$

At this point there are a number of different solutions to $\mathbf{U}$ depending on the method used. In this case the solution is given:

$$\mathbb{U} = \begin{pmatrix} \mathbf{U}^{LL} & \mathbf{U}^{LS} \\ \mathbf{U}^{SL} & \mathbf{U}^{SS} \end{pmatrix} = \begin{pmatrix} \frac{\mathbf{I}}{\sqrt{\mathbf{I} + \mathbf{X}'^{\dagger}\mathbf{X}'}} & -\mathbf{X}'^{\dagger}\frac{\mathbf{I}}{\sqrt{\mathbf{I} + \mathbf{X}'\mathbf{X}'^{\dagger}}} \\ \mathbf{X}'\frac{\mathbf{I}}{\sqrt{\mathbf{I} + \mathbf{X}'^{\dagger}\mathbf{X}'}} & \frac{\mathbf{I}}{\sqrt{\mathbf{I} + \mathbf{X}'\mathbf{X}'^{\dagger}}} \end{pmatrix} \tag{4.39}$$

In order to properly solve for the values of $\mathbf{X}'$ the Dirac-Hamiltonian needs to be solved in the orthonormal basis, this can be done with a standard eigenvalue solution.

$$\mathbb{H}' \begin{pmatrix} \mathbf{C}_{L'}^{+} \\ \mathbf{C}_{S'}^{+} \end{pmatrix} = \begin{pmatrix} \mathbf{C}_{L'}^{+} \\ \mathbf{C}_{S'}^{+} \end{pmatrix} \boldsymbol{\varepsilon}^{+} \tag{4.40}$$

This allows $\mathbf{X}'$ to be found from:

$$\mathbf{X}' = \mathbf{C}_{S'}^{+} \cdot (\mathbf{C}_{L'}^{+})^{-1} \tag{4.41}$$

Up until this point the method for solving the Dirac equation has been identical between ZORA and X2C, the difference occurs when solving for the kinetic energy operator from the relativistic Kohn-Sham DFT equations. The standard kinetic energy operator given by the Kohn-Sham method is given by:

$$\mathrm{T}_{KS} = -\frac{\hbar^2}{2m}\frac{\partial^2}{\partial x^2} \tag{4.42}$$

The Zora method instead gives:

$$\mathrm{T}_{ZORA} = \sigma \cdot p \frac{c^2}{(2c^2 - V_{KS})^2} \sigma \cdot p \tag{4.43}$$

In the subsequent sections we present results where spin-orbit RT-TDDFT is used to simulate X-ray absorption in titania.

4.2 Simulating X-ray Absorption in Solids

The following sections 4.2-4.5 are an excerpt from: “Simulated field-modulated x-ray absorption in titania” [21].

Transition metal oxides possess a wide range of optical [22], electrical [23], and magnetic properties [24-26] that stem from the character and occupations of the *d*-orbitals

[27-30]. These properties can be tailored using external stimuli including electric [31], optical [32], chemical fields [33] due to the changes in the energy/hybridization of the transition metal *d*-orbitals [34, 35]. Subsequently, many modern technologies such as photovoltaics [36, 37], solid-state display panels [38], and non-volatile memory devices [39, 40], that demand charge mobility and reversibility [25] are currently based on transition metal oxides. Recent experiments, for example, have shown that the electronic structure of transition metal oxides can be modulated using electric fields induced by surface ligands, which can be used to tune the optoelectronic properties [33, 41]. For all of these applications, understanding the relationship between applied fields and electronic structure is critical to elucidate the physical mechanisms, and ultimately design new functional inorganic materials. Experimental approaches to this include UV-Vis absorption spectroscopy [42, 43], X-ray photoemission/absorption spectroscopy [41, 44, 45], and magnetic measurements using superconducting quantum interference device (SQUID) [43, 46].

Among these, X-ray absorption near edge spectroscopy (XANES) has emerged as a powerful tool for probing the electronic structure of transition metal oxides [47-49], due to its atomic specificity and ability to capture subtle changes in the unoccupied electronic states (conduction band) [50] that result from changes in lattice geometry [51], oxidation state [52], band spacing [53], and band populations [54]. XANES has been applied to measure changes due to weak fields, such as the effect of surface ligands on the *d*-orbitals of TiO_2 [33], as well as strong field processes such as band-tunneling and transient metallization [55]. Interpreting XANES spectra, however, can be quite

challenging, which necessitates first-principles simulations for relating observed spectra to the underlying electronic structure and/or dynamics.

There are numerous methods for computing XANES spectra for molecules and solids [56-58]. Semi-empirical methods such as crystal-field multiplet (CFM) [59] and charge-transfer multiplet (CTM) [60, 61] can give transition metal spectra that match experiments quite well [33, 62], but require choosing empirical crystal field parameters. Alternatively, one can use ground-state based first-principles (ΔSCF) methods to compute a spectrum directly from the transition between core and valence states. These ΔSCF approaches require some description of the core-hole, which is typically done by constraining the occupancy [63-68]. For the electronic structure method, density functional theory (DFT) [64-66, 69-72] is often used, due to a good tradeoff between accuracy and efficiency. Multiconfigurational methods are also applied to XANES, such as complete/restricted active space SCF (CAS/RASSCF) [67, 73], multireference configuration interaction (MRCI) [74], and multireference coupled cluster (MRCC) [75]. These are especially successful for partially occupied degenerate ground states and partially filled orbitals, but care must be taken in choosing the active space. While SCF-based methods naturally capture relaxation, they may suffer from variational collapse [76]. Additionally, they may require modifications to explicitly enforce orthogonality [77].

Excited-state methods, which do not suffer from these limitations, are also used to compute XANES spectra. Single-determinant excited-state methods such as static exchange (STEX) [78, 79], linear response (LR) [80-82], and real-time (RT) [80, 83-91] time-dependent density functional theory (TDDFT) have been quite successful, but may fail for double excitations and multiplet effects, and often give inaccurate absolute

energies due to incomplete core-hole relaxation [80]. These problems can often be remedied somewhat by using post Hartree-Fock (HF) methods, such as equation-of-motion coupled-cluster (EOM-CC) [75, 92] and real-time EOM-CC [93, 94], which are systematically improvable, but with significantly increased computational cost. Green's function (GW) approaches, such as multiple-scattering with SCF potentials [95, 96], Bethe-Salpeter-Equation (BSE typically with the GW approximation) [97-99], and algebraic diagrammatic construction (ADC) [100] capture relaxation well, but typically require transitions to be calculated separately, which can make them inconvenient for broadband spectroscopy [101].

In particular, XANES calculations of transition metal oxides typically use some form of periodic boundary conditions with either grids or a planewave basis, primarily using DFT [69], multiple scattering [95, 96], and GW/BSE [97-99]. These give a good description of the band structure and reliable spectra. For DFT, however, these basis sets are usually limited to local density (LDA) and generalized gradient (GGA) approximations or Hubbard-correct versions of these functionals (LDA/GGA+U) [102-104]. On the other hand, low concentration of dopants and defects can be challenging, and for practical reasons these basis sets preclude wavefunction-based methods such as hybrid DFT or post-HF techniques. As an alternative, finite simulations can be used, where a cluster is embedded chemically/electrostatically to emulate the bulk [83, 88, 105]. This enables the use of all-electron atom-centered basis sets, which is convenient for inner-shell spectra and allows for efficient evaluation of exchange integrals. However, they can struggle to properly represent long range interactions and can suffer from unphysical finite size effects. Some examples of previous XANES simulations using cluster models include

TiO_2 using DFT [106] and multiple-scattering [107], CaF_2 using ROCIS [106], and iron oxides using MRCI [74]. Finally, relativistic effects can be significant in transition metal oxides, as the spin-orbit (SO) coupling is often on the order of the peak splitting in a XANES spectrum [108]. In TiO_2, for example, the SO splitting in the 2*p* orbitals is roughly 6 eV [33, 34] meaning one cannot simply do a separate L_{III} and L_{II} simulation as for larger Z elements [80].

TDDFT-based methods are convenient for valence properties of condensed-phase systems [109-113] due to the good tradeoff between reasonable computational cost, predictability, and ability to be extended to include SO coupling [19, 85, 88, 108]. Although less common than the valence, TDDFT has also been applied to solid-state XANES including silica[83], alkaline-earth oxides [114], and titania [115]. In this context, atom-centered basis sets and cluster models are especially useful as they obviate the preparation of core holes or transition potentials, and allows for efficient evaluation of hybrid functionals which have been shown to give improved band gaps [116, 117]. Additionally, hybrids have been shown to give better XANES spectra in molecules versus LDA/GGAs, with 50% exact exchange giving the most accurate absolute energies [118]. LR-TDDFT can be challenging due to the convergence issues of the large number of roots required for the calculation of the XANES spectra [119]. Real-time methods, where the density matrix or orbitals are propagated in time, are well-suited to solid-state XANES simulations, as it yields the entire spectrum from valence-to-core transitions without having root convergence issues [8, 120]. Another advantage of using a real-time method, is the ability to simulate non-linear and time-resolved processes [84, 87], such as transient

absorption spectroscopy [121, 122]. The methods developed in this paper were done with this in mind.

This paper demonstrates the use of RT-TDDFT simulations with the inclusion of SO coupling to elucidate the effect of external fields on the electronic structure (XANES spectra) of a prototypical transition metal oxide system, i.e., anatase TiO_2 [123, 124]. First, we develop bulk-mimicking clusters for anatase and validate SO-RT-TDDFT for computing the Ti L-edge XANES spectra. Next, we apply a range of static fields and calculate the field-modified XANES spectra to better understand how observed changes in spectra can be related to changes in the Ti *d*-orbital energy landscape. Ultimately, this work has implications in solar cells [36], (bio)sensing [125, 126], tunable displays [127], and capacitors [128], etc. where application of external fields can be used to modify the optoelectronic properties.

4.3 Theory

All calculations were performed using a customized development version of NWChem[14] with Gaussian-type orbital (GTO) basis sets and relativistic effects described using zeroth order regular approximation (ZORA) [129]. The B3LYP exchange-correlation functional was used for the calculations in this study as it has performed well in previous studies for ground and excited state properties of TiO_2[116, 130]. All the geometry optimizations and similar calculations, along with the XANES calculations, were performed with the following basis sets [131]: Ti atoms were given a Def2-TZVP basis set, O atoms were give a Def2-SVP basis sets, and the pseudo-H atoms were given a 6-31G basis set. In this work, we use bulk-mimicking clusters which are a well-developed approach for weak-field vertical valence and core-level excited states in non-metallic

materials where the excitations are localized in space [132]. Herein, Ti_xO_y clusters were developed using a covalent embedding procedure [105, 110]. The experimental bulk anatase TiO_2 structure was cut to yield a Ti centered finite cluster, which was then "chemically passivated" with pseudo-hydrogen atoms at the boundaries. This is done by replacing the outermost atoms in the cluster by appropriately charged H atoms. In anatase TiO_2, Ti forms a distorted octahedron with the six surrounding O atoms, while O atoms form a trigonal planar structure with the three surrounding Ti atoms. Based on the formal oxidation states of Ti (+4) and O (-2), each Ti atom will share an effective charge of +2/3 and each O atom will possess an effective charge of -2/3 to their neighboring atoms. The boundary pseudo-hydrogen atoms, which replace the outermost Ti atoms, will therefore have an effective charge of +2/3. These charges are independent of the applied electric field. Additionally, by varying the O-H bond lengths one can control how much electron density is donated or withdrawn from the cluster. The O-H bond distance was chosen as 1.0 Å based on previous work [110]. The clusters were then geometry optimized with the interior atoms allowed to move, while pinning the boundary O atoms and fixing the O-H bond lengths and H-O-H angles.

Next, the XANES spectra were computed using the NWChem real-time TDDFT module [86] using a two-component SO approach, similar to previous relativistic RT-TDDFT implementations [19, 82, 88]. A manuscript detailing the validation and technical aspects of this two-component implementation is in preparation [133]. In this approach, the single particle density matrix is propagated in time after broadband pulse excitation. The equation of motion in the von Neumann representation is given by:

$$i\frac{\partial P'(t)}{\partial t} = [F'(t), P'(t)] \tag{4.1}$$

where $\boldsymbol{F}'(t)$ and $\boldsymbol{P}'(t)$ are the Fock and density matrices in the canonical basis[86]. The details regarding the integration of the equation of motion and calculation of the time-advanced Fock matrix are given in ref. [134]. To save computation time, our propagator is constructed via exponential midpoint of the extrapolated (future) Fock matrix without self-consistent iteration.

$$P'(t + \Delta t) = e^{\Omega} P'(t) e^{-\Omega} \tag{4.2}$$

$$\Omega \equiv -iF'(t + \frac{\Delta t}{2})\, \Delta t \tag{4.3}$$

This approximation, which was tested for a few spectra, is valid due to the relatively short time steps, which are required to capture X-ray frequency spectra. The time step used for these calculations is $\Delta t = 7.3 \times 10^{-4}$ fs (0.03 a.u.) and the total time of propagation is 9.7 fs (400 a.u.). The time step was chosen to be short enough to adequately capture the frequency according to the energy range of the XANES spectra. To compute the spectra, the system was excited using a delta-function (broadband) electric field:

$$E(t) = \kappa exp\left[-\frac{(t - t_o)^2}{2w^2}\right] \hat{d} \tag{4.4}$$

For every simulation the field amplitude was taken to be κ = 0.0001 a.u, the center of the pulse was t_o = 20 a.u = 0.48 fs, and the width w = 0.024 fs. $\hat{d} = x, y, z$ denotes the polarization. This electric field is coupled into the Fock matrix in the atomic orbital basis through an external potential (V) by its product with the transition dipole matrix (D), under the assumption of uniform electric field across the system.

$$V(t) = -D.E(t) \tag{4.5}$$

This approximation is valid for relatively low X-ray frequencies studied here. For higher energies, however, quadrupole and higher terms may need to be considered.

A Padé accelerated method of Fourier transform analysis [134] was employed to convert the spectra from time-domain to frequency-domain using only the contributions from the Ti 2*p* core spin-orbitals. This converges much more rapidly with simulation time than conventional Fourier transform of the dipole moment, and also allows one to only include contributions from the L-edge in the spectrum. We checked convergence with simulation time and observed that the spectra were converged for signals longer than 8.5 fs (350 a.u.). An alternative acceleration method is to use a time-correlation function with the energy of the core-level factored out to allow for a larger time step [135].

To compute the spectra, the time-dependent dipole moment is first written as a sum of occupied-virtual pair dipoles:

$$\mu(t) = \mu_o + \sum_{i=1}^{m_{occ}} \sum_{a=m_{occ+1}}^{m} \mu_{ia}(t) \tag{4.6}$$

$$\mu_{ia}(t) = D_{ia}^{MO} P_{ai}^{MO}(t) + D_{ai}^{MO} P_{ia}^{MO}(t) \tag{4.7}$$

where $i = 1, \ldots, m_{occ}$ are the virtual orbitals and $a = m_{occ+1}, \ldots, m$ are the occupied orbitals. These are computed by projecting the density matrix onto the ground state molecular orbitals:

$$D^{MO} = C'^{\dagger}(0) D' C'(0) \tag{4.8}$$

$$P^{MO}(t) = C'^{\dagger}(0) P'(t) C'(0) \tag{4.9}$$

where $C'(0)$ is the eigenvector matrix of the ground state (in the canonical basis). Now the dipole polarizability for each dipole contribution (α_{dd}^{ia}) is obtained by taking Padé approximant to the Fourier transform for each dipole contribution signal separately:

$$\alpha_{dd}^{ia} = \frac{\mu_{dd}^{ia}(\omega) E_d^*(\omega)}{|E_d(\omega)|^2} \tag{4.10}$$

Here, $\hat{d} = x, y, z$ and the dd subscripts denote the on-diagonal part of the polarizability tensor, e.g., xx means x dipole resulting from x polarized kick. The dipole strength function is then computed from the polarizability as:

$$S(\omega) = \frac{4\omega}{3c} Im\left[\alpha_{xx}(\omega) + \alpha_{yy}(\omega) + \alpha_{zz}(\omega)\right] \tag{4.11}$$

Finally, to better match experimental spectra that have lifetimes that generally decrease with increasing energy above the edge, we apply energy dependent broadening to our spectrum separately for both L_{III} and L_{II} edges. This is achieved by fitting the spectrum to a number of Lorentzian curves and then broadening those curves according to τ (E), which takes the form of an exponentially decreasing core-hole lifetime given by:

$$\tau(E) = \tau_o e^{-\alpha(E-E_o)} \tag{4.12}$$

where α has dimensions of inverse energy, E_o stands for edge energy and is equal to 458.1 eV for the L_{III} edge and τ varies from 70-60 s^{-1}. For the L_{II} edge, $E_o = 463.4$ eV and τ varies from 47-25 s^{-1}. Another option for energy dependent broadening is to add a small imaginary potential to the Fock matrix with the values chosen phenomenologically, e.g., exponential in the eigenvalues in the basis of the Kohn Sham orbitals [136]. This results in peaks with increasing widths as you go higher above the edge. However, since the operator is non-Hermitian, strong applied fields will cause significant ionization, which can give unphysical spectra.

4.4 Results and Discussion

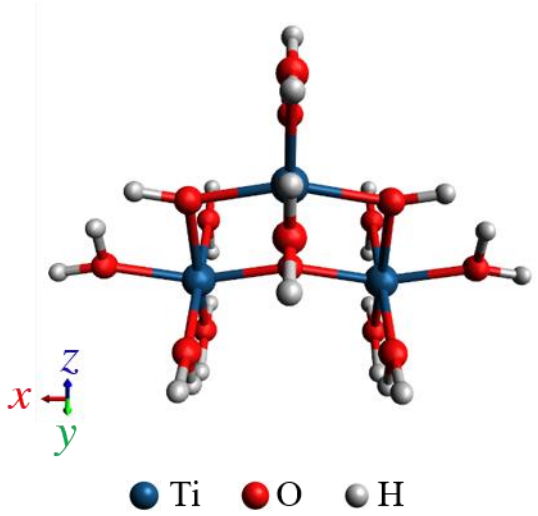

Figure 4.1. $Ti_3O_{14}H_{24}$ bulk-mimicking anatase cluster. Reproduced with permission from J. Chem. Phys. 153, 054110 (2020).

Before computing the effect of electric fields on the XANES spectra, we first validate our approach for the case of anatase TiO_2 without an applied field. To confirm convergence of results with cluster size, we checked the optical gaps and orbital character for a $Ti_9O_{38}H_{60}$ (107 atom) and a smaller $Ti_3O_{14}H_{24}$ (41 atom) cluster (Fig. 4.1) carved from the large one. For convenience, we computed the optical gaps using LR-TDDFT with 10 roots. In principle RT-TDDFT could also be used but would require longer simulation times. The optical gap of the 107-atom cluster was computed to be 3.1 eV with the “valence band” dominated by O 2*p* and the “conduction band” dominated by Ti 3*d* orbitals. The smaller 41 atom cluster had molecular orbitals similar to that of the large cluster with an optical gap of 3.7 eV. This is an overestimate of the experimental value of 3.2 eV [137], likely due to the quantum confinement effects observed in smaller clusters. Although the L-edge spectra should not necessarily depend on the specific value of the optical gap, the value and character of the gap serve as indicators that the cluster is semiconductor-like. Based on these results, the smaller 41 atom cluster adequately

mimics bulk anatase and is thus employed for all subsequent calculations. For the XANES calculations, we use our spin-orbit (SO)-RT-TDDFT version of NWChem since the LR code in NWChem does not have SO coupling.

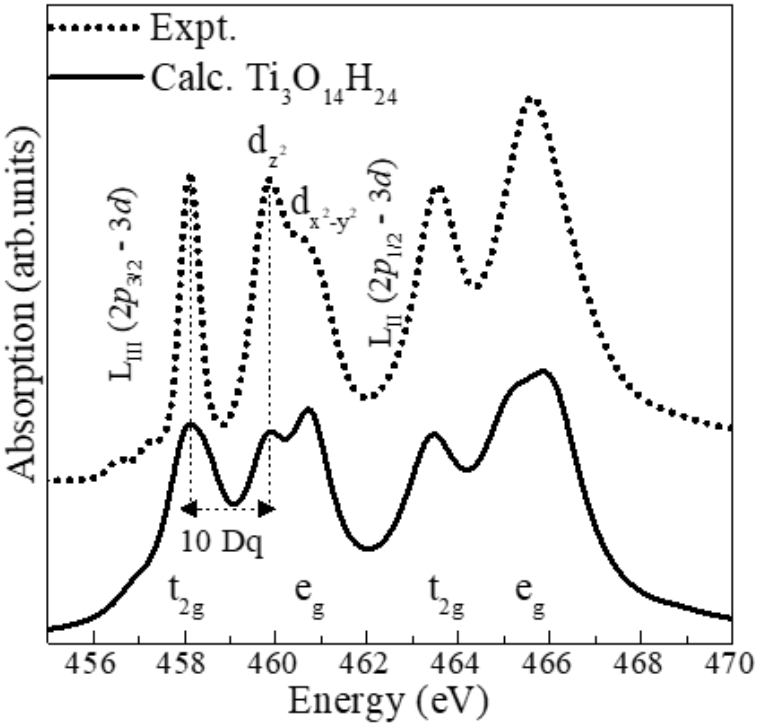

Figure 4.2. Comparison of experimental (dashed) versus calculated (solid) XANES of Ti L-edge for the $Ti_3O_{14}H_{24}$ bulk-mimicking cluster. Reproduced with permission from J. Chem. Phys. 153, 054110 (2020). The experimental spectrum is reproduced with permission from J. Phys. Chem. C 122, 22699 (2018). Copyright 2018 American Chemical Society.

Figure 4.2 shows the resulting Ti L-edge XANES spectrum of the bulk-mimicking $Ti_3O_{14}H_{24}$ anatase cluster. This cluster has 370 basis functions and took approximately two days on using 80 processors to complete the time propagation. To match the experiment, we include energy dependent broadening and then shift our XANES spectrum by +9.33 eV to account for core-hole relaxation effects that are inadequately

captured by TDDFT [138, 139]. Overall, it is observed that there is good agreement with experimental spectrum, including the value of crystal field splitting energy (10 Dq). The two-component SO-RT-TDDFT captures both the L_{III} (Ti $2p_{3/2}$ → Ti $3d$) and L_{II} (Ti $2p_{1/2}$ → Ti $3d$) edges, as well as the energy splitting between them (~6 eV). The peak splitting of the e_g peak in the L_{III} edge is attributed to d_{z^2} and $d_{x^2-y^2}$ orbitals due to the deviation of the Ti from O_h symmetry in anatase [140]. However, in the simulated spectra, the peak intensities of these e_g peaks are reversed, likely due to finite size effects. While RT-TDDFT would be tractable for the 9-Ti (107) atom cluster, we found that the 3-Ti (41) atom cluster already gave adequate agreement with experiment, and thus we did not perform the larger calculation due to computational cost. It would require 3000 processors for the 9-Ti atom cluster, which has 1057 basis functions, to compute the spectra in the same amount of time. This choice of 3-Ti atom cluster is consistent with previously reported restricted open-shell calculations of TiO_2 using the B3LYP functional by Neese and co-workers, who showed that a 3-Ti atom cluster gave nearly converged spectra [106].

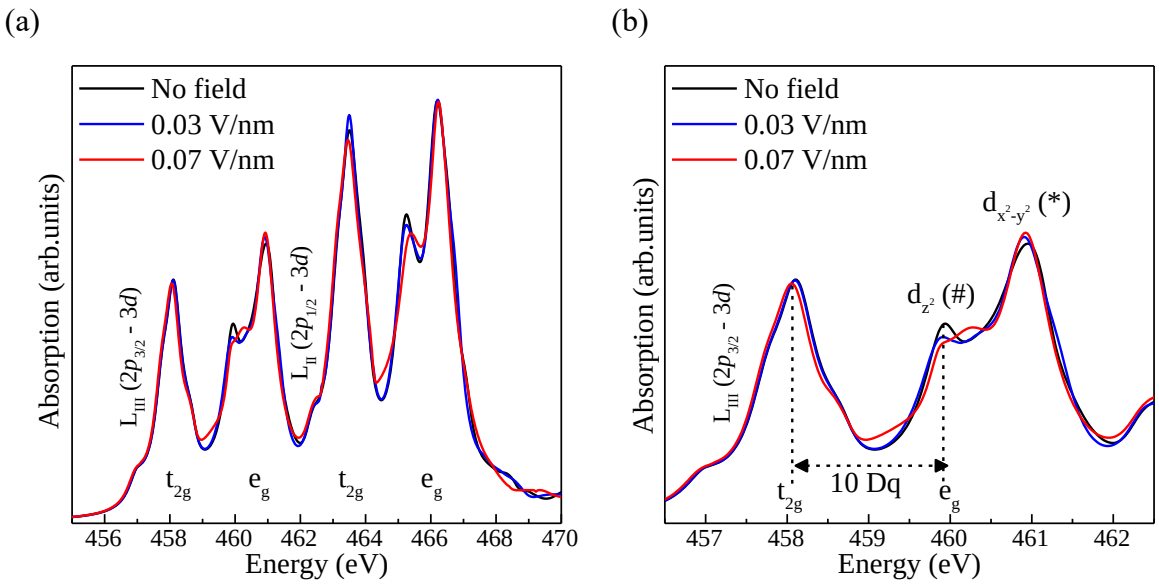

Figure 4.3. (a) Ti $L_{III/II}$ XANES spectra of anatase TiO_2 and (b) expansion of L_{III} edge, showing an increase in the value of 10 Dq with increasing applied electric field. Reproduced with permission from J. Chem. Phys. 153, 054110 (2020).

To elucidate the effects of applied fields on the Ti L-edge XANES spectra and the resulting *d*-orbitals, the system was converged in the ground state in the presence of static electric fields ranging from 0 to 0.07 V/nm applied in the *x*-axis direction. The largest magnitude of field roughly corresponds to half of material's breakdown voltage (~0.14 V/nm) for this cluster, *i.e.*, field at which the band gap disappears. In order to create a quasi-uniform electric field on the $Ti_3O_{14}H_{24}$ cluster, two point charges, with magnitudes ranging from ±43 to 300*e* were separated at a distance of ±100 Å in the *x*-axis of the cluster. Similar calculations with fields applied in *y* and *z*-axes were performed, but did not show any significant differences. To better resolve the spectral features, the Ti L-edge XANES spectra shown in Figure 4.3(a) is uniformly broadened instead of using energy-dependent broadening. Looking at the L_{III} edge (Figure 4.3(b)), first, we notice a subtle

red shift of the onset t_{2g} peak. Second, we observe a splitting of the d_{z^2} (#) peak at higher fields (0.07 V/nm) and third, an increase in the intensity of the $d_{x^2-y^2}$ (*) peak with increasing field is observed. The red shift of the t_{2g} peak at higher fields suggests non-degeneracy of the d_{xy}, d_{yz}, or d_{zx} orbitals [141] upon application of the fields. Analogous to this, the d_{z^2} (#) peak was also observed to split at higher fields. This is phenomenon of *d*-orbital Stark splitting in the presence of applied static fields is similar to that of rare earth 4*f* orbitals, which split in the presence of electromagnetic radiation [142, 143]. An increase in the intensity of the $d_{x^2-y^2}$ (*) features with electric field amplitude is indicative of less hybridization with the *p*-states and thus, higher oscillator dipole strengths [144]. This is attributed to the overlap of the e_g with the ligand *p* states that are along the axes, resulting in a variation of hybridization between the Ti ion and the surrounding ligand. Additionally, the value of crystal field splitting energy (10 Dq), which is calculated as the energy difference between the t_{2g} and d_{z^2} (#) peak in the L_{III} edge, is observed to slightly increase when applied external fields are above a critical strength, in this case between 0.03 and 0.07 V/nm (see SI).

Qualitatively, our calculations are consistent with surface-functionalization experiments on Ni^{2+}-doped TiO_2 films using polarized ligands (μ = ±5 D) [33]. Due to the shallow penetration (< 5 nm) of the ligand-induced fields [145] and soft X-rays [146], as well as the surface segregation of the Ni^{2+} ions, these experimental observations are essentially surface selective. In these experiments, the e_g peak in the Ni L_{II}-edge was observed to increase in intensity with increasing ligand-induced electric field. In this regard, our calculated Ti L_{III}-edge XANES spectra shows a similar effect, albeit at a 10 times stronger field strength compared to the experiments. This is likely due to the partially

filled *d*-orbitals in Ni^{2+} ions, which are strongly influenced by the field than the unoccupied *d*-orbitals in Ti^{4+} [147]. While we cannot directly compare the values of 10 Dq from our calculations (TiO_2) and experiments (Ni^{2+}-doped TiO_2), the 10 Dq calculated from the Ti L_{III}-edge spectra shows a similar trend as the experiments [33, 44, 148] i.e., an increase in its value for fields above 0.03 V/nm.

In these ligand-bonding experiments, the Ni^{2+} L-edge spectra were fit to an empirical model using ligand field multiplet theory [60, 149]. Based on the fitting, the changes in spectra upon ligand-bonding were interpreted as a slight field-induced elongation of the axial bonds around the transition metal ions at the inorganic-organic interface [33]. To differentiate between the roles of electronic effects versus geometry on the spectra, we use a single-Ti atom cluster as an extreme case of possible distortions in the presence of fields. While there was an axial bond distortion upon relaxation of this cluster, these geometry relaxation effects counteracted the electronic effects on the spectra. In other words, the shifts in the spectra due to geometry relaxations are opposite to that of the static field-induced changes. Since the single-Ti atom cluster grossly overestimates the distortions, it is reasonable to conclude that the geometry would be less perturbed in the bulk, and thus having less effect on the spectra. Therefore, the observed changes in the spectra can be attributed to primarily electronic (hybridization) effects.

4.5 Conclusions

In summary, we have developed a spin-orbit real-time TDDFT method to compute the XANES spectra of TiO_2 under the presence of external fields, which captures both the L_{III} and L_{II} edges of Ti. Spin-orbit coupling is crucial for the calculation of L-edge spectra

in first-row transition metal oxide systems as the coupling is of the order of few eVs. For this purpose, bulk-mimicking anatase clusters were developed and the band gap was evaluated to verify the accuracy of the cluster. This finite cluster method offers some advantages over other *ab initio* methods as it uses all electron basis sets and allows for the use of hybrid functionals to improve the quality of XANES spectra. This technique was used to elucidate the field-induced changes in the electronic structure of TiO_2 for static electric fields varying from 0 to 0.07 V/nm. Although it is experimentally challenging to disentangle electronic from geometric field-induced effects, our calculations indicate that fields can modify the electronic structure without geometry distortions. Critically, in the limit that geometry relaxation effects are negligible, these changes in the *d*-orbital hybridization can be probed via XANES. In particular, the onset of the t_{2g} peaks is red shifted and the e_g peaks are blue shifted with increasing fields, along with an increase in the intensity of the $d_{x^2-y^2}$ peak. While these spectral changes are specific to anatase TiO_2 system which has a distorted octahedral Ti^{4+} site (D_{2d}), similar effects are likely to be observed for other transition metal oxides for which first-principles calculations may assist in interpretation.

Appendix. Copyright Information

A.1 Permission to use Chapter 4 text and figures.

AIP PUBLISHING LICENSE
TERMS AND CONDITIONS

Aug 31, 2021

This Agreement between Louisiana State University -- Alexander Meyer ("You") and AIP Publishing ("AIP Publishing") consists of your license details and the terms and conditions provided by AIP Publishing and Copyright Clearance Center.

License Number	5107261220713
License date	Jul 13, 2021
Licensed Content Publisher	AIP Publishing
Licensed Content Publication	Journal of Chemical Physics
Licensed Content Title	Simulated field-modulated x-ray absorption in titania
Licensed Content Author	Pragathi Darapaneni, Alexander M. Meyer, Mykola Sereda, et al
Licensed Content Date	Aug 7, 2020
Licensed Content Volume	153
Licensed Content Issue	5
Type of Use	Thesis/Dissertation
Requestor type	Author (original article)
Format	Print and electronic
Portion	Excerpt (> 800 words)
Will you be translating?	No
Title	Non-Adiabatic Excited State Molecular Dynamics Using Ehrenfest and Modulated X-ray Absorption in Titania
Institution name	Louisiana State University
Expected presentation date	Jul 2021
Portions	I. Introduction II. Methods III. Results IV. Conclusions as well as Fig. 1, Fig. 2 and Fig. 3 on pages 4 and 5
Requestor Location	Louisiana State University 741 Choppin Hall Louisiana State University BATON ROUGE, LA 70803 United States Attn: Louisiana State University
Total	**0.00 USD**

Terms and Conditions

AIP Publishing -- Terms and Conditions: Permissions Uses

AIP Publishing hereby grants to you the non-exclusive right and license to use and/or distribute the Material according to the use specified in your order, on a one-time basis, for the specified term, with a maximum distribution equal to the number that you have ordered. Any links or other content accompanying the Material are not the subject of this license.

1. You agree to include the following copyright and permission notice with the reproduction of the Material:"Reprinted from [FULL CITATION], with the permission of AIP Publishing." For an article, the credit line and permission notice must be printed on the first page of the article or book chapter. For photographs, covers, or tables, the notice may appear with the Material, in a footnote, or in the reference list.
2. If you have licensed reuse of a figure, photograph, cover, or table, it is your responsibility to ensure that the material is

original to AIP Publishing and does not contain the copyright of another entity, and that the copyright notice of the figure, photograph, cover, or table does not indicate that it was reprinted by AIP Publishing, with permission, from another source. Under no circumstances does AIP Publishing purport or intend to grant permission to reuse material to which it does not hold appropriate rights.
You may not alter or modify the Material in any manner. You may translate the Material into another language only if you have licensed translation rights. You may not use the Material for promotional purposes.

3. The foregoing license shall not take effect unless and until AIP Publishing or its agent, Copyright Clearance Center, receives the Payment in accordance with Copyright Clearance Center Billing and Payment Terms and Conditions, which are incorporated herein by reference.
4. AIP Publishing or Copyright Clearance Center may, within two business days of granting this license, revoke the license for any reason whatsoever, with a full refund payable to you. Should you violate the terms of this license at any time, AIP Publishing, or Copyright Clearance Center may revoke the license with no refund to you. Notice of such revocation will be made using the contact information provided by you. Failure to receive such notice will not nullify the revocation.
5. AIP Publishing makes no representations or warranties with respect to the Material. You agree to indemnify and hold harmless AIP Publishing, and their officers, directors, employees or agents from and against any and all claims arising out of your use of the Material other than as specifically authorized herein.
6. The permission granted herein is personal to you and is not transferable or assignable without the prior written permission of AIP Publishing. This license may not be amended except in a writing signed by the party to be charged.
7. If purchase orders, acknowledgments or check endorsements are issued on any forms containing terms and conditions which are inconsistent with these provisions, such inconsistent terms and conditions shall be of no force and effect. This document, including the CCC Billing and Payment Terms and Conditions, shall be the entire agreement between the parties relating to the subject matter hereof.

This Agreement shall be governed by and construed in accordance with the laws of the State of New York. Both parties hereby submit to the jurisdiction of the courts of New York County for purposes of resolving any disputes that may arise hereunder.

V1.2

Questions? customercare@copyright.com or +1-855-239-3415 (toll free in the US) or +1-978-646-2777.

A.2 Permission to use experimental spectrum of Figure 2 in Chapter 4.

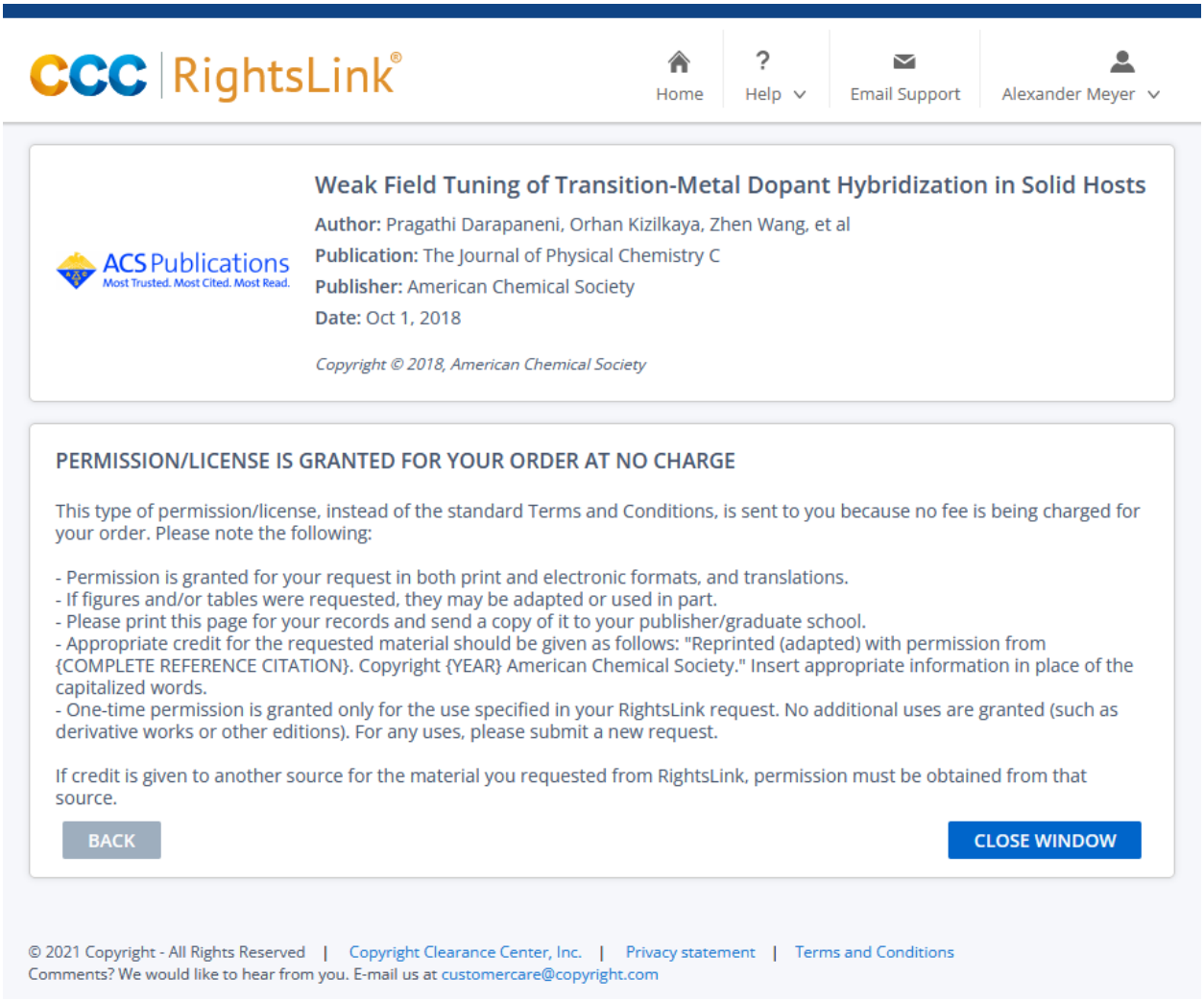

References

[1] J. C. Tully, "Molecular dynamics with electronic transitions," *The Journal of Chemical Physics,* vol. 93, no. 2, pp. 1061-1071, 1990.

[2] X. Li, J. C. Tully, H. B. Schlegel, and M. J. Frisch, "Ab initio Ehrenfest dynamics," *The Journal of chemical physics,* vol. 123, no. 8, p. 084106, 2005.

[3] W. Kohn and L. J. Sham, "Self-consistent equations including exchange and correlation effects," *Physical review,* vol. 140, no. 4A, p. A1133, 1965.

[4] E. Runge and E. K. Gross, "Density-functional theory for time-dependent systems," *Physical Review Letters,* vol. 52, no. 12, p. 997, 1984.

[5] J. I. Fuks, K. Luo, E. D. Sandoval, and N. T. Maitra, "Time-resolved spectroscopy in time-dependent density functional theory: An exact condition," *Physical review letters,* vol. 114, no. 18, p. 183002, 2015.

[6] J. I. Fuks, P. Elliott, A. Rubio, and N. T. Maitra, "Dynamics of charge-transfer processes with time-dependent density functional theory," *The journal of physical chemistry letters,* vol. 4, no. 5, pp. 735-739, 2013.

[7] Y. Wang, K. Lopata, S. A. Chambers, N. Govind, and P. V. Sushko, "Optical absorption and band gap reduction in (fe1–x cr x) 2o3 solid solutions: A first-principles study," *The Journal of Physical Chemistry C,* vol. 117, no. 48, pp. 25504-25512, 2013.

[8] S. Tussupbayev, N. Govind, K. Lopata, and C. J. Cramer, "Comparison of Real-Time and Linear-Response Time-Dependent Density Functional Theories for Molecular Chromophores Ranging from Sparse to High Densities of States," *Journal of Chemical Theory and Computation,* vol. 11, no. 3, pp. 1102-1109, 2015/03/10 2015, doi: 10.1021/ct500763y.

[9] Y. Shinohara, S. Sato, K. Yabana, J.-I. Iwata, T. Otobe, and G. Bertsch, "Erratum:“Nonadiabatic generation of coherent phonons”[J. Chem. Phys. 137, 22A527 (2012)]," *The Journal of Chemical Physics,* vol. 138, no. 2, p. 029903, 2013.

[10] P. Ehrenfest, "Bemerkung über die angenäherte Gültigkeit der klassischen Mechanik innerhalb der Quantenmechanik," *Zeitschrift für Physik,* vol. 45, no. 7-8, pp. 455-457, 1927.

[11] S. A. Fischer, C. T. Chapman, and X. Li, "Surface hopping with Ehrenfest excited potential," *The Journal of chemical physics,* vol. 135, no. 14, p. 144102, 2011.

[12] J. C. Tully, "Perspective: Nonadiabatic dynamics theory," *The Journal of chemical physics,* vol. 137, no. 22, p. 22A301, 2012.

[13] A. Szabo and N. S. Ostlund, *Modern quantum chemistry: introduction to advanced electronic structure theory*. Courier Corporation, 2012.

[14] M. Valiev *et al.*, "NWChem: A comprehensive and scalable open-source solution for large scale molecular simulations," *Computer Physics Communications,* vol. 181, no. 9, pp. 1477-1489, 2010.

[15] W. Press, S. Teukolsky, W. Vetterling, and B. Flannery, "Numerical Recipes The Art of Scientific Computing 3rd Edition, 20 Cambridge University Press," ed, 2007.

[16] E. Livshits and R. Baer, "Time-dependent density-functional studies of the D2 Coulomb explosion," *The Journal of Physical Chemistry A,* vol. 110, no. 27, pp. 8443-8450, 2006.

[17] D. C. Koningsberger and R. Prins, "X-ray absorption: principles, applications, techniques of EXAFS, SEXAFS and XANES," 1987.

[18] D. Haxton and C. McCurdy, "Ultrafast population transfer to excited valence levels of a molecule driven by x-ray pulses," *Physical Review A,* vol. 90, no. 5, p. 053426, 2014.

[19] J. J. Goings, J. M. Kasper, F. Egidi, S. Sun, and X. Li, "Real time propagation of the exact two component time-dependent density functional theory," *The Journal of chemical physics,* vol. 145, no. 10, p. 104107, 2016.

[20] D. Peng, N. Middendorf, F. Weigend, and M. Reiher, "An efficient implementation of two-component relativistic exact-decoupling methods for large molecules," *The Journal of chemical physics,* vol. 138, no. 18, p. 184105, 2013.

[21] P. Darapaneni, A. M. Meyer, M. Sereda, A. Bruner, J. A. Dorman, and K. Lopata, "Simulated field-modulated x-ray absorption in titania," *The Journal of Chemical Physics,* vol. 153, no. 5, p. 054110, 2020.

[22] T. Ofoegbuna, P. Darapaneni, S. Sahu, C. Plaisance, and J. A. Dorman, "Stabilizing the B-site oxidation state in ABO3 perovskite nanoparticles," *Nanoscale,* 10.1039/C9NR04155A vol. 11, no. 30, pp. 14303-14311, 2019, doi: 10.1039/C9NR04155A.

[23] J. Meyer, S. Hamwi, M. Kröger, W. Kowalsky, T. Riedl, and A. Kahn, "Transition metal oxides for organic electronics: energetics, device physics and applications," *Advanced materials,* vol. 24, no. 40, pp. 5408-5427, 2012.

[24] J. Gaudin *et al.*, "Towards simultaneous measurements of electronic and structural properties in ultra-fast x-ray free electron laser absorption spectroscopy experiments," *Scientific Reports,* Article vol. 4, p. 4724, 04/17/online 2014, doi: 10.1038/srep04724.

[25] K. J. Yu, Z. Yan, M. Han, and J. A. Rogers, "Inorganic semiconducting materials for flexible and stretchable electronics," *npj Flexible Electronics,* vol. 1, no. 1, p. 4, 2017/09/26 2017, doi: 10.1038/s41528-017-0003-z.

[26] R. Gupta and A. Pramanik, "Electronic and magnetic properties in Sr1-xLaxRuO3," in *AIP Conference Proceedings*, 2016, vol. 1731, no. 1: AIP Publishing LLC, p. 130055.

[27] N. Bion, F. Epron, M. Moreno, F. Marino, and D. Duprez, "Preferential oxidation of carbon monoxide in the presence of hydrogen (PROX) over noble metals and transition metal oxides: advantages and drawbacks," *Topics in Catalysis,* vol. 51, no. 1-4, p. 76, 2008.

[28] Z. Fang and K. Terakura, "Structural distortion and magnetism in transition metal oxides: crucial roles of orbital degrees of freedom," *Journal of Physics: Condensed Matter,* vol. 14, no. 11, p. 3001, 2002.

[29] W. Deng, X. Ji, Q. Chen, and C. E. Banks, "Electrochemical capacitors utilising transition metal oxides: an update of recent developments," *Rsc Advances,* vol. 1, no. 7, pp. 1171-1178, 2011.

[30] B. Safavinia *et al.*, "Enhancing CexZr1–xO2 Activity for Methane Dry Reforming Using Subsurface Ni Dopants," *ACS Catalysis,* pp. 4070-4079, 2020/03/16 2020, doi: 10.1021/acscatal.0c00203.

[31] J. He *et al.*, "Interfacial and microstructural properties of SrTiO 3 thin films grown on Si (001) substrates," *Journal of applied physics,* vol. 92, no. 12, pp. 7200-7205, 2002.

[32] A. Manivannan, S. K. Myana, K. Miriyala, S. Sahu, and R. Ramadurai, "Low power ovonic threshold switching characteristics of thin GeTe6 films using conductive atomic force microscopy," *Applied Physics Letters,* vol. 105, no. 24, p. 243501, 2014.

[33] P. Darapaneni, O. Kizilkaya, Z. Wang, and J. A. Dorman, "Weak Field Tuning of Transition-Metal Dopant Hybridization in Solid Hosts," *The Journal of Physical Chemistry C,* vol. 122, no. 39, pp. 22699-22708, 2018/10/04 2018, doi: 10.1021/acs.jpcc.8b06069.

[34] P. Darapaneni, N. S. Moura, D. Harry, D. A. Cullen, K. M. Dooley, and J. A. Dorman, "Effect of Moisture on Dopant Segregation in Solid Hosts," *The Journal of Physical Chemistry C,* vol. 123, no. 19, pp. 12234-12241, 2019/05/16 2019, doi: 10.1021/acs.jpcc.9b01067.

[35] R. Watson and L. Bennett, "Transition metals: d-band hybridization, electronegativities and structural stability of intermetallic compounds," *Physical Review B,* vol. 18, no. 12, p. 6439, 1978.

[36] C. Goh, S. R. Scully, and M. D. McGehee, "Effects of molecular interface modification in hybrid organic-inorganic photovoltaic cells," *Journal of applied physics,* vol. 101, no. 11, p. 114503, 2007.

[37] V. Shrotriya, G. Li, Y. Yao, C.-W. Chu, and Y. Yang, "Transition metal oxides as the buffer layer for polymer photovoltaic cells," *Applied Physics Letters,* vol. 88, no. 7, p. 073508, 2006.

[38] J. A. Rogers *et al.*, "like electronic displays: Large-area rubber-stamped plastic sheets of electronics and microencapsulated electrophoretic inks," *Proceedings of the National Academy of Sciences,* vol. 98, no. 9, pp. 4835-4840, 2001.

[39] S. Sahu, A. Manivannan, and U. P. Deshpande, "A systematic evolution of optical band gap and local ordering in Ge1Sb2Te4 and Ge2Sb2Te5 materials revealed by in situ optical spectroscopy," *Journal of Physics D: Applied Physics,* vol. 51, no. 37, p. 375104, 2018.

[40] D. Ielmini, C. Cagli, and F. Nardi, "Resistance transition in metal oxides induced by electronic threshold switching," *Applied Physics Letters,* vol. 94, no. 6, p. 063511, 2009.

[41] P. Darapaneni, O. Kizilkaya, C. Plaisance, and J. A. Dorman, "Adsorption of Polarized Molecules for Interfacial Band Engineering of Doped TiO2 Thin Films," *Langmuir,* 2020/05/05 2020, doi: 10.1021/acs.langmuir.0c00564.

[42] S.-M. Lam, J.-C. Sin, A. Z. Abdullah, and A. R. Mohamed, "Transition metal oxide loaded ZnO nanorods: preparation, characterization and their UV–vis photocatalytic activities," *Separation and Purification Technology,* vol. 132, pp. 378-387, 2014.

[43] A. C. Gluhoi, N. Bogdanchikova, and B. E. Nieuwenhuys, "The effect of different types of additives on the catalytic activity of Au/Al2O3 in propene total oxidation: transition metal oxides and ceria," *Journal of Catalysis,* vol. 229, no. 1, pp. 154-162, 2005.

[44] F. De Groot, J. Fuggle, B. Thole, and G. Sawatzky, "L 2, 3 X-ray-absorption edges of d 0 compounds: K+, Ca 2+, Sc 3+, and Ti 4+ in O h (octahedral) symmetry," *Physical Review B,* vol. 41, no. 2, p. 928, 1990.

[45] T. Ofoegbuna, K. R. Bajgiran, O. Kizilkaya, S. A. J. Thomson, A. T. Melvin, and J. A. Dorman, "Photoluminescence detection of symmetry transformations in low-dimensional ferroelectric ABO3 perovskites," *Journal of Materials Chemistry C,* 10.1039/D0TC01183E 2020, doi: 10.1039/D0TC01183E.

[46] C. Carbone *et al.*, "Natural Fe-oxide and-oxyhydroxide nanoparticles: an EPR and SQUID investigation," *Mineralogy and Petrology,* vol. 85, no. 1-2, pp. 19-32, 2005.

[47] G. S. Henderson, F. M. De Groot, and B. J. Moulton, "X-ray absorption near-edge structure (XANES) spectroscopy," *Reviews in Mineralogy and Geochemistry,* vol. 78, no. 1, pp. 75-138, 2014.

[48] J. Parsons, M. Aldrich, and J. Gardea-Torresdey, "Environmental and biological applications of extended X-ray absorption fine structure (EXAFS) and X-ray absorption near edge structure (XANES) spectroscopies," *Applied Spectroscopy Reviews,* vol. 37, no. 2, pp. 187-222, 2002.

[49] H. Yamashita, M. Matsuoka, K. Tsuji, Y. Shioya, M. Anpo, and M. Che, "In-Situ XAFS, Photoluminescence, and IR Investigations of Copper Ions Included within Various Kinds of Zeolites. Structure of Cu(I) Ions and Their Interaction with CO Molecules," *The Journal of Physical Chemistry,* vol. 100, no. 1, pp. 397-402, 1996/01/01 1996, doi: 10.1021/jp952666z.

[50] V. V. Mesilov *et al.*, "X-ray Diffraction and X-ray Spectroscopy Studies of Cobalt-Doped Anatase TiO2: Co Nanopowders," *The Journal of Physical Chemistry C,* vol. 121, no. 43, pp. 24235-24244, 2017.

[51] E. Gaudry *et al.*, "Structural relaxations around Ti, Cr and Fe impurities in α-Al2O3 probed by X-ray absorption near-edge structure combined with first-principles calculations," *Journal of Physics: Condensed Matter,* vol. 17, no. 36, p. 5467, 2005.

[52] M. Tromp, J. A. van Bokhoven, G. P. van Strijdonck, P. W. van Leeuwen, D. C. Koningsberger, and D. E. Ramaker, "Probing the molecular orbitals and charge redistribution in organometallic (PP) Pd (XX) complexes. A Pd K-edge XANES study," *Journal of the American Chemical Society,* vol. 127, no. 2, pp. 777-789, 2005.

[53] S. Della Longa, A. Soldatov, M. Pompa, and A. Bianconi, "Atomic and electronic structure probed by X-ray absorption spectroscopy: full multiple scattering analysis with the G4XANES package," *Computational Materials Science,* vol. 4, no. 3, pp. 199-210, 1995.

[54] J. Petiau, G. Calas, D. Petitmaire, A. Bianconi, M. Benfatto, and A. Marcelli, "Delocalized versus localized unoccupied 5f states and the uranium site structure in uranium oxides and glasses probed by x-ray-absorption near-edge structure," *Physical Review B,* vol. 34, no. 10, p. 7350, 1986.

[55] M. Schultze *et al.*, "Attosecond band-gap dynamics in silicon," *Science,* vol. 346, no. 6215, pp. 1348-1352, 2014.

[56] J. J. Rehr and R. C. Albers, "Theoretical approaches to x-ray absorption fine structure," *Reviews of modern physics,* vol. 72, no. 3, p. 621, 2000.

[57] N. Ferré, M. Filatov, M. Huix-Rotllant, and C. Adamo, *Density-functional methods for excited states*. Switzerland: Springer International Publishing Switzerland, 2016.

[58] J. Lüder *et al.*, "Theory of L-edge spectroscopy of strongly correlated systems," *Physical Review B,* vol. 96, no. 24, p. 245131, 12/21/ 2017, doi: 10.1103/PhysRevB.96.245131.

[59] F. M. F. de Groot, J. C. Fuggle, B. T. Thole, and G. A. Sawatzky, "2p x-ray absorption of 3d transition-metal compounds: An atomic multiplet description including the crystal field," *Physical Review B,* vol. 42, no. 9, pp. 5459-5468, 09/15/ 1990, doi: 10.1103/PhysRevB.42.5459.

[60] E. Stavitski and F. M. De Groot, "The CTM4XAS program for EELS and XAS spectral shape analysis of transition metal L edges," *Micron,* vol. 41, no. 7, pp. 687-694, 2010.

[61] H. Ikeno, F. M. de Groot, E. Stavitski, and I. Tanaka, "Multiplet calculations of L2, 3 x-ray absorption near-edge structures for 3d transition-metal compounds," *Journal of Physics: Condensed Matter,* vol. 21, no. 10, p. 104208, 2009.

[62] A. Sharma, M. Varshney, H. J. Shin, B.-H. Lee, K. H. Chae, and S. O. Won, "Effect of Cu insertion on structural, local electronic/atomic structure and photocatalyst properties of TiO2, ZnO and Ni(OH)2 nanostructures: XANES-EXAFS study," *Materials Chemistry and Physics,* vol. 191, pp. 129-144, 2017/04/15/ 2017, doi: https://doi.org/10.1016/j.matchemphys.2017.01.008.

[63] Y. Liang, J. Vinson, S. Pemmaraju, W. S. Drisdell, E. L. Shirley, and D. Prendergast, "Accurate x-ray spectral predictions: An advanced self-consistent-field approach inspired by many-body perturbation theory," *Physical review letters,* vol. 118, no. 9, p. 096402, 2017.

[64] D. Cabaret, A. Bordage, A. Juhin, M. Arfaoui, and E. Gaudry, "First-principles calculations of X-ray absorption spectra at the K-edge of 3d transition metals: an electronic structure analysis of the pre-edge," *Physical Chemistry Chemical Physics,* vol. 12, no. 21, pp. 5619-5633, 2010.

[65] D. Cabaret, F. Mauri, and G. S. Henderson, "Oxygen K-edge XANES of germanates investigated using first-principles calculations," *Physical Review B,* vol. 75, no. 18, p. 184205, 2007.

[66] V. Mauchamp, M. Jaouen, and P. Schattschneider, "Core-hole effect in the one-particle approximation revisited from density functional theory," *Physical Review B,* vol. 79, no. 23, p. 235106, 2009.

[67] I. Josefsson *et al.*, "Ab initio calculations of x-ray spectra: Atomic multiplet and molecular orbital effects in a multiconfigurational scf approach to the l-edge

spectra of transition metal complexes," *The journal of physical chemistry letters,* vol. 3, no. 23, pp. 3565-3570, 2012.

[68] M. Taillefumier, D. Cabaret, A.-M. Flank, and F. Mauri, "X-ray absorption near-edge structure calculations with the pseudopotentials: Application to the K edge in diamond and $\ensuremath{\alpha}$-quartz," *Physical Review B,* vol. 66, no. 19, p. 195107, 11/18/ 2002, doi: 10.1103/PhysRevB.66.195107.

[69] T. Okajima, T. Yamamoto, M. Kunisu, S. Yoshioka, I. Tanaka, and N. Umesaki, "Dilute Ga dopant in TiO2 by X-ray absorption near-edge structure," *Japanese journal of applied physics,* vol. 45, no. 9R, p. 7028, 2006.

[70] I. Tanaka and T. Mizoguchi, "First-principles calculations of x-ray absorption near edge structure and energy loss near edge structure: present and future," *Journal of Physics: Condensed Matter,* vol. 21, no. 10, p. 104201, 2009.

[71] S. P. Gao, "Ab initio calculation of ELNES/XANES of BeO polymorphs," *physica status solidi (b),* vol. 247, no. 9, pp. 2190-2194, 2010.

[72] M. Mogi *et al.*, "Theoretical investigation of Al K-edge X-ray absorption spectra of Al, AlN and Al2O3," *Materials transactions,* vol. 45, no. 7, pp. 2031-2034, 2004.

[73] N. C. Tomson *et al.*, "Re-evaluating the Cu K pre-edge XAS transition in complexes with covalent metal–ligand interactions," *Chemical science,* vol. 6, no. 4, pp. 2474-2487, 2015.

[74] M. Sassi, C. I. Pearce, P. S. Bagus, E. Arenholz, and K. M. Rosso, "First-Principles Fe L2, 3-Edge and O K-Edge XANES and XMCD Spectra for Iron Oxides," *The Journal of Physical Chemistry A,* vol. 121, no. 40, pp. 7613-7618, 2017.

[75] J. Brabec, K. Bhaskaran-Nair, N. Govind, J. Pittner, and K. Kowalski, "Communication: Application of state-specific multireference coupled cluster methods to core-level excitations," *Journal of Chemical Physics,* vol. 137, no. 17, p. 171101, 2012.

[76] P. C. De Mello, M. Hehenberger, and M. Zernert, "Converging SCF calculations on excited states," *International Journal of Quantum Chemistry,* vol. 21, no. 1, pp. 251-258, 1982.

[77] W. D. Derricotte and F. A. Evangelista, "Simulation of X-ray absorption spectra with orthogonality constrained density functional theory," *Physical Chemistry Chemical Physics,* vol. 17, no. 22, pp. 14360-14374, 2015.

[78] Y. Mochizuki, H. Koide, T. Imamura, and H. Takemiya, "HF-STEX and RASSCF calculations on nitrogen K-shell X-ray absorption of purine base and its derivative," *Journal of synchrotron radiation,* vol. 8, no. 2, pp. 1003-1005, 2001.

[79] H. Ågren, V. Carravetta, O. Vahtras, and L. G. M. Pettersson, "Direct SCF direct static-exchange calculations of electronic spectra," *Theoretical Chemistry Accounts,* vol. 97, no. 1, pp. 14-40, 1997/10/01 1997, doi: 10.1007/s002140050234.

[80] K. Lopata, B. E. Van Kuiken, M. Khalil, and N. Govind, "Linear-response and real-time time-dependent density functional theory studies of core-level near-edge x-ray absorption," *Journal of chemical theory and computation,* vol. 8, no. 9, pp. 3284-3292, 2012.

[81] W. Liang, S. A. Fischer, M. J. Frisch, and X. Li, "Energy-specific linear response TDHF/TDDFT for calculating high-energy excited states," *Journal of chemical theory and computation,* vol. 7, no. 11, pp. 3540-3547, 2011.

[82] T. Fransson, D. Burdakova, and P. Norman, "K-and L-edge X-ray absorption spectrum calculations of closed-shell carbon, silicon, germanium, and sulfur compounds using damped four-component density functional response theory," *Physical Chemistry Chemical Physics,* vol. 18, no. 19, pp. 13591-13603, 2016.

[83] R. G. Fernando, M. C. Balhoff, and K. Lopata, "X-ray absorption in insulators with non-Hermitian real-time time-dependent density functional theory," *Journal of chemical theory and computation,* vol. 11, no. 2, pp. 646-654, 2015.

[84] Y. Takimoto, F. D. Vila, and J. J. Rehr, "Real-time time-dependent density functional theory approach for frequency-dependent nonlinear optical response in photonic molecules," *The Journal of Chemical Physics,* vol. 127, no. 15, p. 154114, 2007, doi: 10.1063/1.2790014.

[85] C. Pemmaraju, "Valence and core excitons in solids from velocity-gauge real-time TDDFT with range-separated hybrid functionals: An LCAO approach," *Computational Condensed Matter,* vol. 18, p. e00348, 2019.

[86] K. Lopata and N. Govind, "Modeling fast electron dynamics with real-time time-dependent density functional theory: application to small molecules and chromophores," *Journal of chemical theory and computation,* vol. 7, no. 5, pp. 1344-1355, 2011.

[87] F. Ding, B. E. V. Kuiken, B. E. Eichinger, and X. Li, "An efficient method for calculating dynamical hyperpolarizabilities using real-time time-dependent density functional theory," *The Journal of Chemical Physics,* vol. 138, no. 6, p. 064104, 2013, doi: 10.1063/1.4790583.

[88] M. Kadek, L. Konecny, B. Gao, M. Repisky, and K. Ruud, "X-ray absorption resonances near L2,3-edges from real-time propagation of the Dirac–Kohn–Sham density matrix," *Physical Chemistry Chemical Physics,* 10.1039/C5CP03712C vol. 17, no. 35, pp. 22566-22570, 2015, doi: 10.1039/C5CP03712C.

[89] J. Theilhaber, "Ab initio simulations of sodium using time-dependent density-functional theory," *Physical Review B,* vol. 46, no. 20, pp. 12990-13003, 11/15/ 1992, doi: 10.1103/PhysRevB.46.12990.

[90] D. C. Yost, Y. Yao, and Y. Kanai, "Propagation of maximally localized Wannier functions in real-time TDDFT," *The Journal of Chemical Physics,* vol. 150, no. 19, p. 194113, 2019, doi: 10.1063/1.5095631.

[91] K. Yabana and G. F. Bertsch, "Time-dependent local-density approximation in real time," *Physical Review B,* vol. 54, no. 7, pp. 4484-4487, 08/15/ 1996, doi: 10.1103/PhysRevB.54.4484.

[92] J. Liu, D. Matthews, S. Coriani, and L. Cheng, "Benchmark Calculations of K-Edge Ionization Energies for First-Row Elements Using Scalar-Relativistic Core–Valence-Separated Equation-of-Motion Coupled-Cluster Methods," *Journal of Chemical Theory and Computation,* vol. 15, no. 3, pp. 1642-1651, 2019/03/12 2019, doi: 10.1021/acs.jctc.8b01160.

[93] D. R. Nascimento and A. E. DePrince, "Linear Absorption Spectra from Explicitly Time-Dependent Equation-of-Motion Coupled-Cluster Theory," *Journal of Chemical Theory and Computation,* vol. 12, no. 12, pp. 5834-5840, 2016/12/13 2016, doi: 10.1021/acs.jctc.6b00796.

[94] D. R. Nascimento and A. E. DePrince, "Simulation of Near-Edge X-ray Absorption Fine Structure with Time-Dependent Equation-of-Motion Coupled-Cluster Theory," *The Journal of Physical Chemistry Letters,* vol. 8, no. 13, pp. 2951-2957, 2017/07/06 2017, doi: 10.1021/acs.jpclett.7b01206.

[95] A. Bianconi, M. Dell'Ariccia, P. J. Durham, and J. B. Pendry, "Multiple-scattering resonances and structural effects in the x-ray-absorption near-edge spectra of Fe II and Fe III hexacyanide complexes," *Physical Review B,* vol. 26, no. 12, pp. 6502-6508, 12/15/ 1982, doi: 10.1103/PhysRevB.26.6502.

[96] A. Ankudinov, B. Ravel, J. Rehr, and S. Conradson, "Real-space multiple-scattering calculation and interpretation of x-ray-absorption near-edge structure," *Physical Review B,* vol. 58, no. 12, p. 7565, 1998.

[97] E. L. Shirley, "Bethe–Salpeter treatment of X-ray absorption including core-hole multiplet effects," *Journal of electron spectroscopy and related phenomena,* vol. 144, pp. 1187-1190, 2005.

[98] K. Gilmore *et al.*, "Efficient implementation of core-excitation Bethe–Salpeter equation calculations," *Computer Physics Communications,* vol. 197, pp. 109-117, 2015.

[99] J. Vinson and J. Rehr, "Ab initio Bethe-Salpeter calculations of the x-ray absorption spectra of transition metals at the L-shell edges," *Physical Review B,* vol. 86, no. 19, p. 195135, 2012.

[100] J. Wenzel, M. Wormit, and A. Dreuw, "Calculating X-ray Absorption Spectra of Open-Shell Molecules with the Unrestricted Algebraic-Diagrammatic Construction Scheme for the Polarization Propagator," *Journal of Chemical Theory and Computation,* vol. 10, no. 10, pp. 4583-4598, 2014/10/14 2014, doi: 10.1021/ct5006888.

[101] X. Blase, I. Duchemin, and D. Jacquemin, "The Bethe–Salpeter equation in chemistry: relations with TD-DFT, applications and challenges," *Chemical Society Reviews,* 10.1039/C7CS00049A vol. 47, no. 3, pp. 1022-1043, 2018, doi: 10.1039/C7CS00049A.

[102] K. Tatsumi *et al.*, "Local atomic and electronic structures around Mg and Al dopants in ${\text{LiNiO}}_{2}$ electrodes studied by XANES and ELNES and first-principles calculations," *Physical Review B,* vol. 78, no. 4, p. 045108, 07/16/ 2008, doi: 10.1103/PhysRevB.78.045108.

[103] V. I. Anisimov, F. Aryasetiawan, and A. I. Lichtenstein, "First-principles calculations of the electronic structure and spectra of strongly correlated systems: theLDA+Umethod," *Journal of Physics: Condensed Matter,* vol. 9, no. 4, pp. 767-808, 1997/01/27 1997, doi: 10.1088/0953-8984/9/4/002.

[104] P. Canepa, E. Schofield, A. V. Chadwick, and M. Alfredsson, "Comparison of a calculated and measured XANES spectrum of α-Fe2O3," *Physical Chemistry Chemical Physics,* 10.1039/C1CP00034A vol. 13, no. 28, pp. 12826-12834, 2011, doi: 10.1039/C1CP00034A.

[105] J. Sauer, "Molecular models in ab initio studies of solids and surfaces: from ionic crystals and semiconductors to catalysts," *Chemical Reviews,* vol. 89, no. 1, pp. 199-255, 1989.

[106] D. Maganas, S. DeBeer, and F. Neese, "Restricted open-shell conFuration interaction cluster calculations of the L-edge x-ray absorption study of TiO2 and CaF2 solids," *Inorganic chemistry,* vol. 53, no. 13, pp. 6374-6385, 2014.

[107] M. F. Ruiz-Lopez and A. Munoz-Paez, "A theoretical study of the XANES spectra of rutile and anatase," *Journal of Physics: Condensed Matter,* vol. 3, no. 45, pp. 8981-8990, 1991/11/11 1991, doi: 10.1088/0953-8984/3/45/019.

[108] O. Bunău and Y. Joly, "Time-dependent density functional theory applied to x-ray absorption spectroscopy," *Physical Review B,* vol. 85, no. 15, p. 155121, 04/12/ 2012, doi: 10.1103/PhysRevB.85.155121.

[109] L. K. Dash, N. Vast, P. Baranek, M.-C. Cheynet, and L. Reining, "Electronic structure and electron energy-loss spectroscopy of ${\mathrm{ZrO}}_{2}$ zirconia," *Physical Review B,* vol. 70, no. 24, p. 245116, 12/20/ 2004, doi: 10.1103/PhysRevB.70.245116.

[110] N. Govind, K. Lopata, R. Rousseau, A. Andersen, and K. Kowalski, "Visible Light Absorption of N-Doped TiO2 Rutile Using (LR/RT)-TDDFT and Active Space EOMCCSD Calculations," *The Journal of Physical Chemistry Letters,* vol. 2, no. 21, pp. 2696-2701, 2011/11/03 2011, doi: 10.1021/jz201118r.

[111] F. Sottile *et al.*, "TDDFT from molecules to solids: The role of long-range interactions," *International Journal of Quantum Chemistry,* vol. 102, no. 5, pp. 684-701, 2005, doi: 10.1002/qua.20486.

[112] D. C. Yost and Y. Kanai, "Electronic stopping for protons and $\ensuremath{\alpha}$ particles from first-principles electron dynamics: The case of silicon carbide," *Physical Review B,* vol. 94, no. 11, p. 115107, 09/06/ 2016, doi: 10.1103/PhysRevB.94.115107.

[113] S. A. Sato, Y. Shinohara, T. Otobe, and K. Yabana, "Dielectric response of laser-excited silicon at finite electron temperature," *Physical Review B,* vol. 90, no. 17, p. 174303, 11/11/ 2014, doi: 10.1103/PhysRevB.90.174303.

[114] R. De Francesco, M. Stener, and G. Fronzoni, "TDDFT Calculations of NEXAFS Spectra of Model Systems for SO2 Adsorbed on the MgO (100) Surface," *The Journal of Physical Chemistry C,* vol. 111, no. 36, pp. 13554-13563, 2007/09/01 2007, doi: 10.1021/jp072710y.

[115] G. Fronzoni, R. De Francesco, M. Stener, and M. Causà, "X-ray Absorption Spectroscopy of Titanium Oxide by Time Dependent Density Functional Calculations," *The Journal of Physical Chemistry B,* vol. 110, no. 20, pp. 9899-9907, 2006/05/01 2006, doi: 10.1021/jp057353a.

[116] J. Muscat, A. Wander, and N. Harrison, "On the prediction of band gaps from hybrid functional theory," *Chemical Physics Letters,* vol. 342, no. 3-4, pp. 397-401, 2001.

[117] T. Bredow and A. R. Gerson, "Effect of exchange and correlation on bulk properties of MgO, NiO, and CoO," *Physical Review B,* vol. 61, no. 8, pp. 5194-5201, 02/15/ 2000, doi: 10.1103/PhysRevB.61.5194.

[118] P. Verma and R. J. Bartlett, "Increasing the applicability of density functional theory. V. X-ray absorption spectra with ionization potential corrected exchange and correlation potentials," *The Journal of chemical physics,* vol. 145, no. 3, p. 034108, 2016.

[119] J. Brabec *et al.*, "Efficient Algorithms for Estimating the Absorption Spectrum within Linear Response TDDFT," *Journal of Chemical Theory and Computation,* vol. 11, no. 11, pp. 5197-5208, 2015/11/10 2015, doi: 10.1021/acs.jctc.5b00887.

[120] J. Sun, J. Song, Y. Zhao, and W.-Z. Liang, "Real-time propagation of the reduced one-electron density matrix in atom-centered Gaussian orbitals: Application to

absorption spectra of silicon clusters," *The Journal of Chemical Physics,* vol. 127, no. 23, p. 234107, 2007, doi: 10.1063/1.2805396.

[121] S. A. Sato, H. Hübener, U. De Giovannini, and A. Rubio, "Ab Initio Simulation of Attosecond Transient Absorption Spectroscopy in Two-Dimensional Materials," *Applied Sciences,* vol. 8, no. 10, p. 1777, 2018.

[122] M. Chen and K. Lopata, "First-Principles Simulations of X-ray Transient Absorption for Probing Attosecond Electron Dynamics," *Submitted,* 2020.

[123] D. B. Hamal, J. A. Haggstrom, G. L. Marchin, M. A. Ikenberry, K. Hohn, and K. J. Klabunde, "A multifunctional biocide/sporocide and photocatalyst based on titanium dioxide (TiO2) codoped with silver, carbon, and sulfur," *Langmuir,* vol. 26, no. 4, pp. 2805-2810, 2009.

[124] X. Feng, K. Shankar, O. K. Varghese, M. Paulose, T. J. Latempa, and C. A. Grimes, "Vertically aligned single crystal TiO2 nanowire arrays grown directly on transparent conducting oxide coated glass: synthesis details and applications," *Nano letters,* vol. 8, no. 11, pp. 3781-3786, 2008.

[125] K. R Bajgiran, P. Darapaneni, A. T. Melvin, and J. A. Dorman, "Effects of Weak Electric Field on the Photoluminescence Behavior of Bi3+-Doped YVO4:Eu3+ Core–Shell Nanoparticles," *The Journal of Physical Chemistry C,* vol. 123, no. 20, pp. 13027-13035, 2019/05/23 2019, doi: 10.1021/acs.jpcc.9b01872.

[126] K. R. Bajgiran, J. A. Dorman, and A. T. Melvin, "Dipole-Modulated Downconversion Nanoparticles as Label-Free Biological Sensors," *ACS Sensors,* vol. 5, no. 1, pp. 29-33, 2020/01/24 2020, doi: 10.1021/acssensors.9b02204.

[127] Z. Li, P. Desai, R. B. Akins, G. Ventouris, and D. Voloschenko, "Electrically tunable color for full-color reflective displays," in *Liquid Crystal Materials, Devices, and Applications VIII*, 2002, vol. 4658: International Society for Optics and Photonics, pp. 7-13.

[128] J. R. Miller and P. Simon, "Electrochemical capacitors for energy management," *science,* vol. 321, no. 5889, pp. 651-652, 2008.

[129] P. Nichols, N. Govind, E. J. Bylaska, and W. A. De Jong, "Gaussian Basis Set and Planewave Relativistic Spin− Orbit Methods in NWChem," *Journal of chemical theory and computation,* vol. 5, no. 3, pp. 491-499, 2009.

[130] F. Labat, P. Baranek, and C. Adamo, "Structural and electronic properties of selected rutile and anatase TiO2 surfaces: an ab initio investigation," *Journal of Chemical Theory and Computation,* vol. 4, no. 2, pp. 341-352, 2008.

[131] B. P. Pritchard, D. Altarawy, B. Didier, T. D. Gibson, and T. L. Windus, "New Basis Set Exchange: An Open, Up-to-Date Resource for the Molecular Sciences

Community," *Journal of chemical information and modeling,* vol. 59, no. 11, pp. 4814-4820, 2019.

[132] E. A. Carter, "Challenges in modeling materials properties without experimental input," *Science,* vol. 321, no. 5890, pp. 800-803, 2008.

[133] K. Lopata, M. Sereda, B. Poulter, M. Khalil, Y. Zhang, and N. Govind, "UV-Vis and X-ray L2,3 Edge Spectroscopy fromTwo-Component Relativistic Real-TimeTime-Dependent Density Functional Theory," *In Preparation,* 2020.

[134] A. Bruner, D. LaMaster, and K. Lopata, "Accelerated broadband spectra using transition dipole decomposition and Padé approximants," *Journal of chemical theory and computation,* vol. 12, no. 8, pp. 3741-3750, 2016.

[135] A. J. Lee, F. D. Vila, and J. J. Rehr, "Local time-correlation approach for calculations of x-ray spectra," *Physical Review B,* vol. 86, no. 11, p. 115107, 09/07/ 2012, doi: 10.1103/PhysRevB.86.115107.

[136] K. Lopata and N. Govind, "Near and above ionization electronic excitations with non-hermitian real-time time-dependent density functional theory," *Journal of chemical theory and computation,* vol. 9, no. 11, pp. 4939-4946, 2013.

[137] T. Umebayashi, T. Yamaki, H. Itoh, and K. Asai, "Band gap narrowing of titanium dioxide by sulfur doping," *Applied Physics Letters,* vol. 81, no. 3, pp. 454-456, 2002.

[138] S. DeBeer George, T. Petrenko, and F. Neese, "Prediction of iron K-edge absorption spectra using time-dependent density functional theory," *The Journal of Physical Chemistry A,* vol. 112, no. 50, pp. 12936-12943, 2008.

[139] N. A. Besley and F. A. Asmuruf, "Time-dependent density functional theory calculations of the spectroscopy of core electrons," *Physical Chemistry Chemical Physics,* vol. 12, no. 38, pp. 12024-12039, 2010.

[140] G. Henderson, X. Liu, and M. Fleet, "A Ti L-edge X-ray absorption study of Ti-silicate glasses," *Physics and Chemistry of Minerals,* vol. 29, no. 1, pp. 32-42, 2002.

[141] M. Mochizuki and M. Imada, "Orbital-Spin Structure and Lattice Coupling in R T i O 3 where R= L a, P r, N d, and S m," *Physical review letters,* vol. 91, no. 16, p. 167203, 2003.

[142] M. Vaithiyanathan, K. R. Bajgiran, P. Darapaneni, N. Safa, J. A. Dorman, and A. T. Melvin, "Luminescent nanomaterials for droplet tracking in a microfluidic trapping array," *Analytical and Bioanalytical Chemistry,* journal article vol. 411, no. 1, pp. 157-170, January 01 2019, doi: 10.1007/s00216-018-1448-1.

[143] Y. Wang, P. Darapaneni, O. Kizilkaya, and J. A. Dorman, "Role of Ce in Manipulating the Photoluminescence of Tb Doped Y2Zr2O7," *Inorganic Chemistry,* vol. 59, no. 4, pp. 2358-2366, 2020/02/17 2020, doi: 10.1021/acs.inorgchem.9b03226.

[144] M. Guo, L. K. Sørensen, M. G. Delcey, R. V. Pinjari, and M. Lundberg, "Simulations of iron K pre-edge X-ray absorption spectra using the restricted active space method," *Physical Chemistry Chemical Physics,* vol. 18, no. 4, pp. 3250-3259, 2016.

[145] M. Moreno, M. Barriuso, and J. Aramburu, "The dependence of 10Dq upon the metal–ligand distance, R, for transition-metal complexes. What is its microscopic origin?," *International journal of quantum chemistry,* vol. 52, no. 4, pp. 829-835, 1994.

[146] M. Abbate *et al.*, "Probing depth of soft x-ray absorption spectroscopy measured in total-electron-yield mode," *Surface and Interface Analysis,* vol. 18, no. 1, pp. 65-69, 1992, doi: 10.1002/sia.740180111.

[147] M. Lenglet, "Ligand field spectroscopy and chemical bonding in Cr3+-, Fe3+-, Co2+- and Ni2+-containing oxidic solids: Influence of the inductive effect of the competing bonds and magnetic interactions on the degree of covalency of the 3d M–O bonds," *Materials Research Bulletin,* vol. 35, no. 4, pp. 531-543, 2000/03/01/ 2000, doi: https://doi.org/10.1016/S0025-5408(00)00243-9.

[148] S. P. Cramer *et al.*, "Ligand field strengths and oxidation states from manganese L-edge spectroscopy," *Journal of the American Chemical Society,* vol. 113, no. 21, pp. 7937-7940, 1991/10/01 1991, doi: 10.1021/ja00021a018.

[149] E. Stavitski and F. de Groot, "CTM4XAS 5.2 Manual," ed: Version, 2008.

Vita

Alexander M. Meyer graduated from University of California Irvine in 2010 with a B.S. in chemistry. After graduation he worked as a chemist, developing methods for testing pharmaceuticals. He is currently a Ph.D. candidate in the Lopata research group at Louisiana State University in Baton Rouge, LA. His research interests include electron and nuclear dynamics, with a focus on solid state materials.